

## DETECTING ISOLATED SPECTRUM OF TRANSFER AND KOOPMAN OPERATORS WITH FOURIER ANALYTIC TOOLS

GARY FROYLAND AND CECILIA GONZÁLEZ-TOKMAN

School of Mathematics and Statistics  
University of New South Wales  
Sydney, NSW, 2052, Australia

ANTHONY QUAS

Department of Mathematics and Statistics  
University of Victoria  
Victoria, BC, Canada, V8W 3R4

(Communicated by the associate editor name)

**ABSTRACT.** The isolated spectrum of transfer operators is known to play a critical role in determining mixing properties of piecewise smooth dynamical systems. The so-called Dellnitz-Froyland ansatz places isolated eigenvalues in correspondence with structures in phase space that decay at rates slower than local expansion can account for. Numerical approximations of transfer operator spectrum are often insufficient to distinguish isolated spectral points, so it is an open problem to decide to which eigenvectors the ansatz applies. We propose a new numerical technique to identify the isolated spectrum and large-scale structures alluded to in the ansatz. This harmonic analytic approach relies on new stability properties of the Ulam scheme for both transfer and Koopman operators, which are also established here. We demonstrate the efficacy of this scheme in metastable one- and two-dimensional dynamical systems, including those with both expanding and contracting dynamics, and explain how the leading eigenfunctions govern the dynamics for both real and complex isolated eigenvalues.

### 1. Introduction.

**1.1. Background and overview.** The isolated spectrum of transfer operators plays a critical role in determining mixing properties of dynamical systems. After [11], transfer operator techniques have been applied in the study of almost-invariant sets in molecular dynamics [38] as well as ocean dynamics [18]. The so-called Dellnitz-Froyland ansatz initially proposed in [10], asserts that eigenvectors of transfer operators associated to isolated spectral values encode global dynamical features, such as structures responsible for slower than expected mixing rates.

---

2010 *Mathematics Subject Classification.* Primary: 37M25; Secondary: 37E05.

*Key words and phrases.* Transfer operators, Koopman operators, isolated spectrum, Ulam's method, metastability, mix-norms.

GF is supported by an Australian Research Council Future Fellowship. CGT acknowledges support from ARC Discovery Project DP110100068. AQ's research is partially supported by NSERC. AQ also acknowledges support from ARC for travel to UNSW and thanks UNSW for accommodating him.

These structures are associated with metastability phenomena, which have also been studied via the transfer operator approach in recent years [31, 19, 14, 20, 13, 1].

Despite being linear and bounded, transfer operators often have very complicated spectra, without any isolated eigenvalues, when considered in spaces such as  $L^p(\text{Leb})$  or the space of continuous functions; see e.g. [3, Theorem 2.5]. The efforts to better understand the behavior of transfer operators have led to the study of their actions on more general Banach spaces. For example, spaces of smooth functions  $C^k$ , the space of bounded variation functions  $BV$  with its higher dimensional generalizations, Sobolev spaces of fractional order  $\mathcal{H}_p^t$ , and others. The general strategy behind the choice of such a space is to ensure that the transfer operator  $\mathcal{L}$  restricted to it is *quasi-compact*. Roughly speaking,  $\mathcal{L}$  is quasi-compact if, outside a disk of radius  $\rho_e < 1$ , called *essential spectral radius*, the spectrum of  $\mathcal{L}$  consists of isolated eigenvalues of finite multiplicity, including 1. See §2.2 for more details.

The part of the spectrum corresponding to eigenvalues of magnitude 1 has received significant attention in the literature. A recent general result in this direction is [5, Theorem 14]<sup>1</sup>, which implies that under rather general assumptions – including piecewise expanding and hyperbolic settings – eigenvectors of eigenvalue 1 correspond to *physical* invariant measures<sup>2</sup>, that the multiplicity of 1 is given by the (finite) number of ergodic such measures, and that their basins cover Lebesgue almost every point of the state space. Also, there are finitely many eigenvalues of magnitude 1, all of which are roots of unity. Thus, there exists  $k \geq 1$  such that 1 is the only eigenvalue of modulus 1 for the transfer operator of  $\mathcal{L}^k$ . Early results in this direction, including some explicit bounds on the multiplicity of 1 are [25, 36, 22, 37, 9]<sup>3</sup>. It is also possible in some cases to give estimates [24] and even explicit formulas [29] for the essential spectral radius  $\rho_e$ .

However, it is in general an open problem to give bounds on the *number* of isolated eigenvalues of magnitude greater than  $\rho_e$ . In fact, the general theory only provides the existence of at least one, and at most countably many of them. The existence of non-trivial eigenvalues (that is, of magnitude strictly less than 1) was known for specific examples in the context of piecewise expanding affine Markov maps [2], and general techniques for constructing such maps were developed in [10]. In the setting of smooth expanding maps, the first example that appeared in the literature is due to Keller and Rugh [32].

The transition from invariant to almost-invariant components is a delicate phenomenon, which can be observed in relatively simple systems. Consider the piecewise expanding map with three invariant subintervals shown in Figure 1. Figure 2 shows numerical approximations to the top 5 eigenvectors of the transfer operator (top row) and its adjoint, the Koopman operator (bottom row) for the piecewise expanding map of Figure 1.

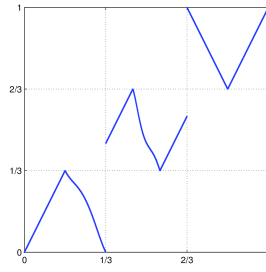


FIGURE 1. Graph of system with three invariant components, corresponding to (14) with parameters  $\epsilon = 0$  and  $\delta = 0$ .

<sup>1</sup>We refer the reader to [6, 12] for earlier results along these lines.

<sup>2</sup>That is, invariant measures whose basins include a set of positive Lebesgue measure. In the expanding setting, physical measures are absolutely continuous with respect to Lebesgue.

<sup>3</sup>It is also worth pointing out that some exceptions to this decomposition exist in dimensions greater than 1, even in the expanding setting, as the multiplicity of 1 may be infinite [41, 8].

In this case it is rather straightforward to

- (i) qualitatively distinguish the first three eigenvectors from the last two; and (ii) identify the three invariant components from the level sets of the first three Koopman eigenvectors.

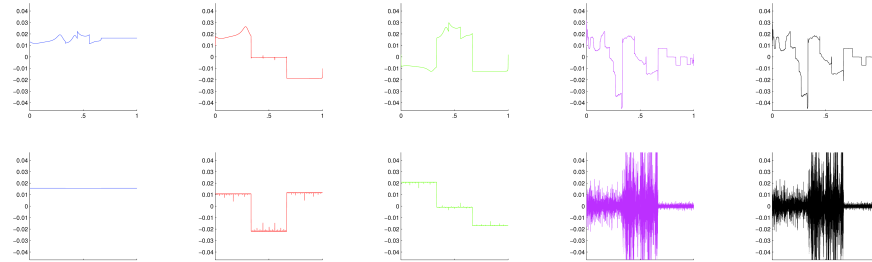


FIGURE 2. Numerical approximation to the top 5 eigenvectors of transfer (top) and Koopman (bottom) operators of a map with three invariant sub-intervals (Figure 1).

In contrast, consider Figure 3(a) depicting a relatively small perturbation of the previous map, in which there are no invariant sets of positive Lebesgue measure other than the whole interval, and invariance of the three sub-intervals is turned into almost-invariance. Figure 4 shows the corresponding eigenvectors. In this case, questions such as “*what are the almost-invariant sets?*” and “*how many of them are there?*” become harder to answer by inspecting the eigenfunctions. The situation is even worse in multi-dimensional systems with a mixture of expanding and contracting behavior, as the corresponding eigenfunctions tend to be highly irregular along stable directions. This may even be the case for systems with an *a priori* clear presence of almost-invariant sets.

In this paper we propose an algorithm for determining non-trivial isolated spectrum of transfer operators numerically. We also exhibit a harmonic analytic strategy to identify almost-invariant sets, based on the Dellnitz-Froyland ansatz. The rough idea is that by smoothing eigenvectors, it is possible to differentiate their underlying large-scale features. The pertinence of this approach in our setting is elaborated in §1.2.

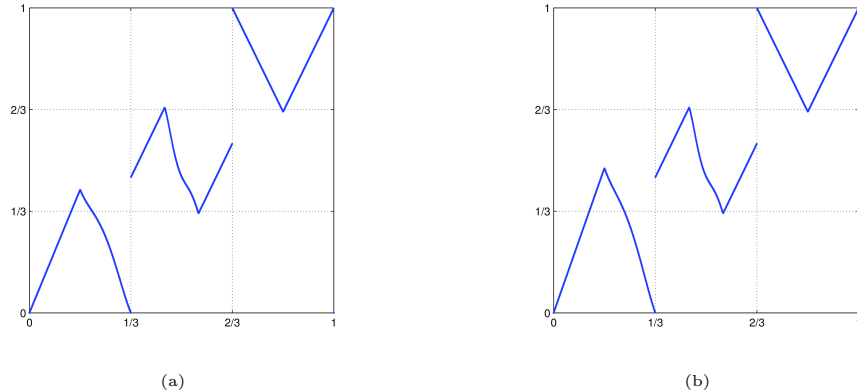


FIGURE 3. Graphs of systems with three almost-invariant components (14), with parameters  $\epsilon = .01$  and (a)  $\delta = 0.1$ , (b)  $\delta = 0.2$ .

To illustrate the scope of the proposed techniques, we present numerical experiments for one- and two-dimensional systems. The one-dimensional systems are piecewise expanding, and the two-dimensional ones have non-uniformly expanding and contracting directions. An advantage of the approach in the present paper is that it is useful even when dealing with one *fixed* discretization of the transfer operator. Indeed, it does not depend on the possibility of observing asymptotic behavior over a sequence of finer and finer approximations. This is an important fact, given that the construction of Ulam matrices with high resolution is still a time-consuming process.

We expect that this work will contribute useful tools for the study of mixing and metastability phenomena in more complicated systems, where rigorous theory may still be out of reach. Furthermore, we expect the ideas developed here can be extended to the case of random systems, such as those studied in [16, 21] but we do not pursue this approach further in the present work.

**1.2. Approach.** Our approach exploits prior knowledge about the regularity of transfer and Koopman eigenvectors, as well as a strong type of convergence of Ulam's numerical approximation scheme to detect isolated spectrum and almost-invariant sets in dynamical systems with *hyperbolicity* features.

When a non-singular system  $T : M \rightarrow M$  has several invariant components of positive Lebesgue measure, the corresponding eigenvectors of the Koopman operator  $\mathcal{L}^*$  are particularly simple: they correspond to integration with respect to Lebesgue measure on the different invariant sets. This is a direct consequence of the fact that  $\text{Leb}(f) = \text{Leb}(\mathcal{L}f)$ . Indeed, if  $A \subset M$  is invariant under  $T$ , then the linear functional  $f \mapsto \int_A f d\text{Leb}$  is fixed under  $\mathcal{L}^*$ , when restricted to an appropriate space.

The strategy behind the numerical tests developed in this work is in some sense reminiscent of the above phenomenon. It is worth remarking that one can in principle observe a similar behavior for transfer operator eigenvectors, after rescaling all of them by the top one (the invariant density). This procedure may be useful in some situations, but it introduces numerical issues in cases where the invariant density is very far from uniform.

We rely on stability of Koopman eigenvectors, including control of certain regularity properties. It is worth pointing out that Koopman operators are receiving their own attention in the applied literature; see the recent article [7]. From a theoretical perspective, Koopman operators are often more complicated to deal with than transfer operators, even in relatively simple systems such as expanding maps. A reason for this is that if one wants to exploit functional analytical properties

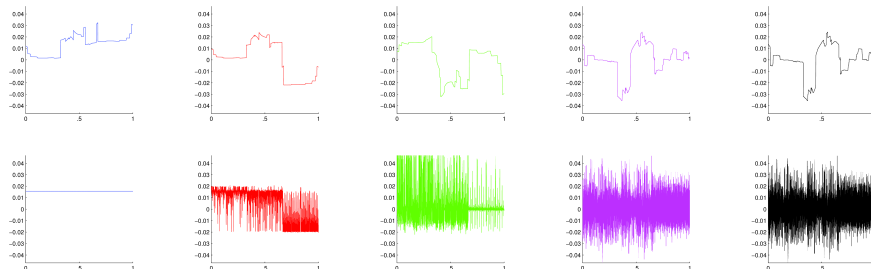


FIGURE 4. Numerical approximation to top 5 eigenvectors of the transfer operator (top) and Koopman operator (bottom) of a map with three almost-invariant sub-intervals (Figure 3(a)).

such as quasi-compactness, Koopman operators must be considered as linear operators on a space of distributions. Since rigorous results along these lines are, to our knowledge, not present in the literature, we develop the necessary theory as well. In particular, *a rigorous convergence result is established in the context of piecewise smooth expanding one-dimensional maps*, building on technology developed by Keller and Liverani [30].

More precisely, we establish a rigorous convergence result in the context of fractional Sobolev norms, which have been used in the transfer operator literature by Baladi and coauthors [4, 5]. It is worth remarking that in the applied literature on mixing systems, it has become customary to employ a similar type of Sobolev norm to measure mixing. These are the so-called mix-norms, introduced in [34] and recently reviewed in [40]. These two sets of norms are essentially related by duality: in the presence of expansion, the transfer operator behaves nicely on fractional Sobolev spaces of order  $t > 0$ , while the mix-norms are equivalent to fractional Sobolev norms of order  $t < 0$ .

One way to define fractional Sobolev spaces is via properties of their Fourier transforms. This characterization is the one that allows us to connect the theory with harmonic-analysis ideas, such as smoothing, to identify almost-invariant sets. This point of view also allows us to make use of existing harmonic-analysis tools for numerical implementations.

**1.3. Outline.** The necessary theoretical tools, including concepts and results about quasi-compactness and stability, are presented in §2. A stability result for the Ulam approximation scheme, underpinning the upcoming numerical tests, is presented in §3. A new test for the detection of non-trivial isolated eigenvalues of transfer and Koopman operators is presented in §4. This test also allows for a visualization of almost-invariant sets of a dynamical system as level sets of a suitable transformation of the non-trivial isolated Koopman eigenvectors, in the spirit of the Dellnitz-Froyland ansatz. The efficacy of this approach is demonstrated in a variety of examples, including a family of metastable one-dimensional piecewise expanding maps in §4.1, and two-dimensional systems in §4.2.

## 2. Theoretical preliminaries.

**2.1. Transfer and Koopman operators.** Consider a dynamical system  $T : M \circlearrowright$ , acting on a compact manifold, possibly with boundary. The *Koopman operator*  $\mathcal{L}^*$  associated to  $T$  arises naturally as the dynamical action of  $T$  on bounded functions: Given  $f : M \rightarrow \mathbb{R}$ ,  $\mathcal{L}^*(f)$  is defined as  $f \circ T$ . The *Perron-Frobenius* or *transfer operator* associated to  $T$  is defined by duality. Provided  $M$  is equipped with a probability measure  $\mu$  and  $T$  is non-singular with respect to  $\mu$  (that is,  $\mu(A) = 0$  iff  $\mu(T^{-1}(A)) = 0$ ), one can define  $\mathcal{L} : L^1(\mu) \circlearrowleft$  as the pre-dual of  $\mathcal{L}^* : L^\infty(\mu) \circlearrowright$ , defined above. Thus, for every  $f \in L^1(\mu)$  and  $g \in L^\infty(\mu)$ , we have the relation  $\int_M \mathcal{L}f \cdot g \, d\mu = \int_M f \cdot \mathcal{L}^*g \, d\mu = \int_X f \cdot g \circ T \, d\mu$ . Throughout this work,  $\mu$  will be the normalized Lebesgue measure, denoted by  $\text{Leb}$ .

While in the context of expanding and hyperbolic dynamical systems the analytical theory has been developed mostly for the transfer operator, we are primarily concerned with eigenvectors of the Koopman operator, as discussed in §1.2. In particular, we are interested in those eigenvectors associated to non-trivial isolated eigenvalues. Here, non-trivial means of magnitude strictly between the essential spectral radius  $\rho_e$  and 1.

Fortunately, duality allows one to transfer several useful properties from a transfer operator  $\mathcal{L}$  to the corresponding Koopman operator  $\mathcal{L}^*$ . One known example is quasi-compactness, which has been extensively exploited in the study of transfer operators. This is the topic of §2.2. Also, stability results may be translated from transfer to Koopman operators, although care is needed in the interpretation of convergence in a distribution space. This will be treated in §2.3.

**2.2. Quasi-compactness.** Let  $\mathcal{L} : X \curvearrowright$  be a bounded linear operator on a Banach space. The *spectral radius* of  $\mathcal{L}$  is defined as  $\rho(\mathcal{L}) := \lim_{n \rightarrow \infty} \|\mathcal{L}^n\|^{1/n}$ .  $\mathcal{L}$  is called *quasi-compact* when there exists a number  $0 \leq \rho_e(\mathcal{L}) < \rho(\mathcal{L})$ , called the *essential spectral radius* of  $\mathcal{L}$ , and  $1 \leq l \leq \infty$  so that the spectrum of  $\mathcal{L}$  outside the disc of radius  $\rho_e(\mathcal{L})$  consists of isolated points  $r_1, \dots, r_l$ , all of which are eigenvalues of  $\mathcal{L}$  of finite (algebraic and geometric) multiplicity<sup>4</sup>. We will refer to these as *isolated eigenvalues* of  $\mathcal{L}$ .

When  $\mathcal{L}$  is quasi-compact, it may be written as follows:

$$\mathcal{L} = \sum_{i=1}^l (r_i P_i + D_i) + \mathcal{R}, \quad (1)$$

where  $P_i$  is the eigenprojection and  $D_i$  the eigennilpotent corresponding to  $r_i$ , [3, §1.3], [28, §III.5]. Furthermore,  $\rho(\mathcal{R}) < |r_l|$ , and the following relations are satisfied.

$$P_i P_j = \delta_{ij} P_i, \quad P_i D_i = D_i P_i = D_i, \quad (\mathcal{L} - r_i) P_i = D_i, \quad P_i \mathcal{R} = \mathcal{R} P_i = 0. \quad (2)$$

In particular, these imply that

$$\mathcal{L}^n = \sum_{i=1}^l (r_i P_i + D_i)^n + \mathcal{R}^n. \quad (3)$$

Hence, quasi-compactness allows for the spectral analysis of the non-trivial isolated eigenvalues, which, together with eigenvalues of magnitude 1, are dynamically the most important.

The adjoint of  $\mathcal{L} : X \curvearrowright$ ,  $\mathcal{L}^* : X^* \curvearrowright$ , acts on the dual of  $X$  which is normed by  $\|\phi\|_* := \sup_{f \in X, \|f\| \leq 1} |\phi(f)|$ .  $\mathcal{L}^*$  is defined by duality, via  $\mathcal{L}^*(\phi)f := \phi(\mathcal{L}f)$ . Quasi-compactness of  $\mathcal{L}$  implies quasi-compactness of  $\mathcal{L}^*$ ; this is an exercise in [3]. In particular, if  $\mathcal{L}$  satisfies (1), then  $\mathcal{L}^*$  may be written as follows:

$$\mathcal{L}^* = \sum_{i=1}^l (\bar{r}_i P_i^* + D_i^*) + \mathcal{R}^*. \quad (4)$$

Notice that the adjoint of a projection is always a projection, and the adjoint of a nilpotent is always nilpotent. Furthermore,  $\|\mathcal{R}^*\|_* = \|\mathcal{R}\|$  [28, III.3], and therefore  $\rho(\mathcal{R}^*) = \rho(\mathcal{R}) < |r_l|$ . The adjoint version of relations (2) holds also.

### 2.3. Stability.

---

<sup>4</sup>Although  $l$  may be infinite, we will pretend it is finite. This does not represent any loss of generality in our analysis, as it amounts to possibly enlarging the value of  $\rho_e(\mathcal{L})$  slightly, making sure it does not exceed the spectral radius of  $\mathcal{L}$ ,  $\rho(\mathcal{L})$ . We also order  $r_1, \dots, r_l$  in non-increasing order of magnitude.

**2.3.1. The Keller-Liverani result and a dual version.** It is known that, in many interesting cases, operators  $\mathcal{L}_\epsilon$  arising from small perturbations of a Perron-Frobenius operator  $\mathcal{L}_0 : (X, \|\cdot\|) \curvearrowright$  do not converge in the norm topology. That is, it often happens that  $\|\mathcal{L}_\epsilon - \mathcal{L}_0\| \not\rightarrow 0$  as  $\epsilon \rightarrow 0$ .

Frequently, it is the case that  $\lim_{\epsilon \rightarrow 0} \|\mathcal{L}_\epsilon - \mathcal{L}_0\| = 0$ , where the *triple norm*  $\|\cdot\|$  is defined in terms of two norms on  $X$ , as follows. Let  $\mathcal{L} \in L(X, \|\cdot\|)$  be a bounded linear operator that extends to a bounded linear operator on a Banach space  $(Y, |\cdot|)$ , such that  $X \subset Y$  and  $|x| \leq \|x\|$  for every  $x \in X$ . Then,  $\|\mathcal{L}\|$  is the norm of  $\mathcal{L} : (X, \|\cdot\|) \rightarrow (Y, |\cdot|)$ . That is,

$$\|\mathcal{L}\| := \sup_{\|x\| \leq 1} |\mathcal{L}x|. \quad (5)$$

Thus, the triple norm is weaker than the operator norm on  $(X, \|\cdot\|)$ .

Keller and Liverani [30] showed that, under certain conditions on  $\{\mathcal{L}_\epsilon\}_{\epsilon \geq 0}$ , whenever  $\lim_{\epsilon \rightarrow 0} \|\mathcal{L}_\epsilon - \mathcal{L}_0\| = 0$ , and the  $\mathcal{L}_\epsilon$  are quasi-compact, then the isolated eigenvalues of  $\mathcal{L}_0$  and its associated eigenvectors enjoy stability properties. In particular, they established the following.

**Theorem 2.1** ([30]). *Let  $\mathcal{L}_0 = \mathcal{L} : X \curvearrowright$  be a quasi-compact operator satisfying (1). Suppose  $\{\mathcal{L}_\epsilon\}_{\epsilon \geq 0}$  are quasi-compact operators on  $(X, \|\cdot\|)$  such that  $\lim_{\epsilon \rightarrow 0} \|\mathcal{L}_\epsilon - \mathcal{L}_0\| = 0$ . Under the extra assumptions (ii)-(iv) of [30]<sup>5</sup>, there exists  $\delta > 0$  such that if  $\epsilon > 0$  is sufficiently small, for every  $1 \leq j \leq l$ , the projections*

$$\Pi_j^{\epsilon, \delta} := \frac{1}{2\pi i} \int_{\partial B_\delta(r_j)} (z - \mathcal{L}_\epsilon)^{-1} dz$$

are well defined, independent of the choice of  $\delta$  for sufficiently small  $\delta$ , and satisfy the property

$$\lim_{\epsilon \rightarrow 0} \|\Pi_j^{\epsilon, \delta} - \Pi_j^{0, \delta}\| = 0. \quad (6)$$

Furthermore,  $\text{rank}(\Pi_j^{\epsilon, \delta}) = \text{rank}(\Pi_j^{0, \delta})$ . Also, for  $|r| > \alpha$  (see condition (iii)), let

$$\Pi_r^\epsilon := \frac{1}{2\pi i} \int_{\partial B_r(0)} (z - \mathcal{L}_\epsilon)^{-1} dz.$$

Then,

$$\lim_{\epsilon \rightarrow 0} \|\Pi_r^\epsilon - \Pi_r^0\| = 0, \quad (7)$$

and there exists  $K = K(\delta, r) > 0$  such that for all  $\epsilon > 0$  sufficiently small and for all  $n \in \mathbb{N}$ ,  $\|\mathcal{L}_\epsilon^n \Pi_r^\epsilon\| \leq Kr^n$ .

This result may be translated into a convergence statement about Koopman operators, via the following lemma.

**Lemma 2.2.** *Let  $(X, \|\cdot\|)$  and  $(Y, |\cdot|)$  be Banach spaces with  $X \subset Y$  and  $|x| \leq \|x\|$  for every  $x \in X$ . Let  $\mathcal{L} \in L(X, \|\cdot\|)$  be a bounded linear operator that extends to a bounded linear operator on  $(Y, |\cdot|)$ , and let  $\|\mathcal{L}\|$  be defined as in (5). Then,  $\mathcal{L}^* \in L(X^*, \|\cdot\|_*) \cap L(Y^*, |\cdot|_*)$ , and  $\|\mathcal{L}^*\|_* \leq \|\mathcal{L}\|$ , where  $\|\mathcal{L}^*\|_* := \sup_{\phi \in Y^*, |\phi|_* \leq 1} \|\mathcal{L}^* \phi\|_*$ .*

---

<sup>5</sup>(ii) is  $|\mathcal{L}_\epsilon^n| \leq C_1 M^n$  for some  $C_1, M > 0$ ; (iii) is  $\|\mathcal{L}_\epsilon^n f\| \leq C_2 \alpha^n \|f\| + C_3 |f|$  for some  $0 < \alpha < 1$  and  $C_2, C_3 > 0$ ; then (iv), regarding the *residual* spectrum of  $\mathcal{L}_\epsilon$ , automatically holds whenever the embedding  $(X, \|\cdot\|) \hookrightarrow (Y, |\cdot|)$  is compact.

*Proof.* The first statement is straightforward from the definitions. The last statement may be checked as follows.

$$\begin{aligned} \|\mathcal{L}^*\|_* &= \sup_{\phi \in Y^*, |\phi|_* \leq 1} \|\mathcal{L}^* \phi\|_* = \sup_{\phi \in Y^*, |\phi|_* \leq 1} \sup_{f \in X, \|f\| \leq 1} |\phi(\mathcal{L} f)| \\ &\leq \sup_{\phi \in Y^*, |\phi|_* \leq 1} \sup_{g \in Y, |g|=1} \|\mathcal{L}\| |\phi(g)| = \|\mathcal{L}\|. \end{aligned}$$

□

Combining Theorem 2.1 with Lemma 2.2, we get the following.

**Corollary 2.3.** *Under the conditions of Theorem 2.1,*

$$\lim_{\epsilon \rightarrow 0} \|(\Pi_i^{\epsilon, \delta})^* - (\Pi_i^{0, \delta})^*\|_* = 0. \quad (8)$$

Furthermore, the operators  $(\Pi_i^{\epsilon, \delta})^*$  correspond to the sum of eigenprojections onto eigenspaces of  $\mathcal{L}_\epsilon^*$  of eigenvalues inside  $B_\delta(\bar{r}_i)$ .

*Proof.* The first statement follows directly from Lemma 2.2. The last statement follows from [28, III, Theorem 6.22]. □

**2.3.2. Stability in the Grassmannian distance.** In order to extract some concrete and useful information from the previous stability results, let us introduce some terminology. Given  $A, B \subset X$  closed subspaces, let  $d_{|\cdot|}(A, B)$  be the Grassmannian distance between  $A$  and  $B$ , that is, the Hausdorff distance between the unit balls in  $A$  and  $B$ ,

$$d_{|\cdot|}(A, B) := \max \left( \sup_{a \in A, |a|=1} \inf_{b \in B, |b|=1} |a - b|, \sup_{b \in B, |b|=1} \inf_{a \in A, |a|=1} |a - b| \right). \quad (9)$$

**Proposition 2.4.** *Suppose (6) holds. Let  $E_i^\epsilon := \Pi_i^{\epsilon, \delta} X$ , and assume<sup>6</sup>  $\dim E_i^\epsilon = \dim E_i^0$ . Then,*

$$\lim_{\epsilon \rightarrow 0} d_{|\cdot|}(E_i^0, E_i^\epsilon) = 0. \quad (10)$$

**Remark 2.5.** *Equation (10) implies the following.*

- (I) *If  $f \in E_i^0$ , then there exist  $f_\epsilon \in E_i^\epsilon$  such that  $\lim_{\epsilon \rightarrow 0} |f - f_\epsilon| = 0$ .*
- (II) *If  $\lim_{n \rightarrow \infty} \epsilon_n = 0$ ,  $f_n \in E_i^{\epsilon_n}$  and  $\lim_{n \rightarrow \infty} f_n = f$  (in the norm  $|\cdot|$ ), then  $f \in E_i^0$ .*

*Proof of Proposition 2.4.* Let  $s_i = \sup_{x \in E_i \setminus \{0\}} \frac{\|x\|}{|x|}$ . Since  $E_i$  is finite-dimensional,  $s_i > 0$ . Let us estimate the first term of the right hand side of (9). Let  $\tau_\epsilon = \|\Pi_i^{\epsilon, \delta} - \Pi_i^{0, \delta}\|$ . Let  $x \in E_i^0, |x|=1$ . Then,

$$|\Pi_i^{\epsilon, \delta}(x) - \Pi_i^{0, \delta}(x)| = |\Pi_i^{\epsilon, \delta}(x) - x| \leq \tau_\epsilon \|x\|.$$

Thus, by the reverse triangle inequality,  $|\Pi_i^{\epsilon, \delta}(x)| \geq 1 - \tau_\epsilon \|x\|$ . So,  $\inf_{y \in E_i^\epsilon, |y|=1} |x - y| \leq |x - \Pi_i^{\epsilon, \delta}(x)| / |\Pi_i^{\epsilon, \delta}(x)| \leq 4\tau_\epsilon \|x\|$ , provided  $\tau_\epsilon s_i < 1/2$ . Thus,

$$\sup_{x \in E_i^0, |x|=1} \inf_{y \in E_i^\epsilon, |y|=1} |x - y| \leq 4\tau_\epsilon s_i. \quad (11)$$

Using the fact that  $\dim E_i^\epsilon = \dim E_i^0$ , [27, Lemma 213] shows that if  $\tau_\epsilon$  is sufficiently small and (11) holds, then  $\sup_{x \in E_i^\epsilon, |x|=1} \inf_{y \in E_i^0, |y|=1} |x - y| \leq 8\tau_\epsilon s_i$ . Thus,  $d_{|\cdot|}(E_i^0, E_i^\epsilon) \leq 8\tau_\epsilon s_i$ , and the conclusion follows. □

---

<sup>6</sup>This always holds for sufficiently small  $\epsilon$  in the Keller-Liverani setup; see Theorem 2.1.

An immediate consequence of Proposition 2.4 and Corollary 2.3 is the following.

**Corollary 2.6.** *Suppose the assumptions of Proposition 2.4 hold. Let  $(E_i^\epsilon)^* := (\Pi_i^{\epsilon,\delta})^* X^*$ . Then,*

$$\lim_{\epsilon \rightarrow 0} d_{\|\cdot\|_*}((E_i^0)^*, (E_i^\epsilon)^*) = 0. \quad (12)$$

**2.3.3. Interpreting convergence of Koopman eigenvectors.** The results of the previous sections provide a rigorous way to extend convergence results for isolated eigenvalues of the Perron-Frobenius operator available in the literature to rigorous statements about convergence – in a suitable sense – of eigenvectors of Koopman operators, also known as Koopman modes.

This “suitable sense” is in general neither pointwise, nor in a sense of closeness in some normed function space, such as  $L^p$  or  $C^k$ , so it may not be evident to the eye when plotting numerically computed eigenvectors. This issue is exemplified by the fact that the second and third plots of the second rows of Figures 2 and 4, despite looking completely different, are indeed close in some sense.

Closeness of Koopman modes should be interpreted in some distributional sense. For a simple example, consider the doubling map  $T$  on  $S^1 \subset \mathbb{C}$ , given by  $T(z) = z^2$ . Start with any, say,  $C^1$  function  $g : S^1 \rightarrow \mathbb{R}$ . Then,  $(\mathcal{L}^*)^k(g) = g \circ T^k$  is given by  $z \mapsto g(z^{2^k})$ . This is typically a very oscillatory function for large  $k$ . However, when regarded as a distribution in the dual of  $C^1$ , the sequence  $(\mathcal{L}^*)^k(g)$  converges to the linear functional  $f \mapsto a \int f \, d\text{Leb}$ , where  $a = \int g \, d\text{Leb}$ . Indeed, for every  $f \in C^1$ , as  $k \rightarrow \infty$ , the mixing property of  $T$  ensures that

$$\int (\mathcal{L}^*)^k(g) f \, d\text{Leb} = \int g \circ T^k \cdot f \, d\text{Leb} \rightarrow \int g \, d\text{Leb} \int f \, d\text{Leb}.$$

A more general setup, which allows us to treat maps with discontinuities and is also numerically tractable with Fourier analysis tools, is introduced in §3.

**3. The Ulam scheme in fractional Sobolev spaces.** The Ulam method [42] provides a way of approximating the transfer operator  $\mathcal{L}$  of a dynamical system  $T : M \curvearrowright$  via a sequence of finite-rank operators  $\mathcal{L}_k$ , each taking values on piecewise constant functions. They are defined as follows.

For each  $k \in \mathbb{N}$ , let  $\mathcal{P}_k = \{B_1, \dots, B_k\}$  be a partition of  $M$  into  $k$  subsets of positive Lebesgue measure, called bins. Let  $\mathbb{E}_k$  be given by the formula

$$\mathbb{E}_k(f) = \sum_{j=1}^k \frac{1}{\text{Leb}(B_j)} \left( \int 1_{B_j} f \, d\text{Leb} \right) 1_{B_j}.$$

Let  $\mathcal{L}_k := \mathbb{E}_k \mathcal{L}$ . The  $k \times k$  matrix representing  $\mathcal{L}_k$  in the ordered basis  $\{1_{B_1}, \dots, 1_{B_k}\}$  is called the Ulam matrix. When these matrices are available, the left and right eigenvectors provide approximations for Perron-Frobenius and Koopman operator eigenvectors, respectively.

Fractional Sobolev spaces are well-studied Banach spaces which were introduced to the transfer operator literature in [5]. They are of interest for this work because they make the Ulam scheme compatible with the Keller-Liverani stability technology, as will be established in Theorem 3.1 for the one-dimensional case. Furthermore, these spaces are characterized in terms of Fourier transforms, and this fact will allow us to gain insight into the corresponding eigenvectors via numerical tests in §4. They are defined as follows.

Let  $t, p \in \mathbb{R}$ . Let  $\mathcal{H}_p^t$  be the subset of the fractional Sobolev space with parameters  $p$  and  $t$  on  $\mathbb{R}^d$ . That is,  $\mathcal{H}_p^t$  is the space of tempered distributions  $f$  such that

$$\mathcal{F}^{-1}(m_t \mathcal{F}(f)) \in L^p(\mathbb{R}^d),$$

where  $\mathcal{F}$  denotes the Fourier transform, and  $m_t(\xi) := (1 + |\xi|^2)^{\frac{t}{2}} =: \langle \xi \rangle^{t/2}$ . The norm on  $\mathcal{H}_p^t$  is given by

$$\|f\|_{\mathcal{H}_p^t} := \|\mathcal{F}^{-1}(m_t \mathcal{F}(f))\|_p. \quad (13)$$

In applications to transfer operators, the specific choice of parameters  $p$  and  $t$  depends on the map. In particular, they satisfy  $0 < t < \frac{1}{p}$ , where  $t$  is a smoothness parameter, and it can not be larger than the smoothness of the (derivative of the) map.

Given a manifold  $M$ , one can construct fractional Sobolev spaces on  $M$ ,  $\mathcal{H}_p^t(M)$ , via charts, and different choices of charts give rise to the same space, with equivalent norms; see e.g. [5]. The main theoretical result of this section is the following.

**Theorem 3.1** (Convergence of the Ulam scheme in fractional Sobolev spaces). *Let  $0 < \alpha \leq 1$ , and  $0 < t' < t < \min(\alpha, \frac{1}{p}) < 1$ .<sup>7</sup> Let  $T : I \circlearrowright$  be a piecewise  $C^{1+\alpha}$  sufficiently expanding map<sup>8</sup>, and let  $\mathcal{L} : \mathcal{H}_p^t \circlearrowright$  be the transfer operator of  $T$ .<sup>9</sup> Let  $\{\mathcal{L}_n\}_{n \in \mathbb{N}}$  be the operators arising from the Ulam scheme with bins taken to be  $n$  subintervals of uniform length, corresponding to  $\epsilon_n := 1/n$ . Then, the stability results of §2.3 hold. In particular, the isolated eigenvalues and eigenspaces of  $\mathcal{L}_n$  and  $\mathcal{L}_n^*$  converge (in  $\mathcal{H}_p^{t'}$  and  $\mathcal{H}_p^{t'*} = \mathcal{H}_q^{-t}$ , respectively) to those of  $\mathcal{L}$  and  $\mathcal{L}^*$ .*

The proof of Theorem 3.1 is deferred until Appendix A.

**Remark 3.2.** *When  $T$  is piecewise  $C^2$ , a result analogous to Theorem 3.1 is valid with fractional Sobolev spaces replaced by the space of functions of bounded variation,  $BV \subset L^1$ . Indeed, stability of the Ulam scheme is established in [30], and the arguments of §2.3 ensure stability of the Koopman operator on  $BV^*$ . The main reason for us to focus on the less classical setting of fractional Sobolev spaces is that their duals – which are themselves fractional Sobolev spaces – are more manageable than  $BV^*$ .*

**4. Numerical tests for detecting isolated eigenvalues and large-scale almost-invariant sets.** In this section we present a numerical test, which exploits Fourier analytical properties of the *right* eigenvectors of (row-stochastic) Ulam matrices to detect the isolated spectrum of transfer (and Koopman) operators.

We consider matrix approximations to transfer operators arising from the Ulam scheme introduced in §3. In the setting of Theorem 3.1, the leading left and right eigenvectors of such matrices yield approximations to the isolated eigenvectors of the original transfer and Koopman operators, respectively. These approximations are close in the sense of fractional Sobolev norms, defined in (13).

Suppose  $w_j$  is a small perturbation of an isolated eigenvector  $W_j$  of a Koopman operator  $\mathcal{L}^*$ , in  $\mathcal{H}_q^{-t}$ . Then, by definition, applying the smoothing transformation

<sup>7</sup>Then, the  $\mathcal{H}_p^t(I)$  norm is stronger than  $\mathcal{H}_p^{t'}(I)$ . We will drop the dependence of the space on the manifold, as it will be clear from the context.

<sup>8</sup>Explicit bounds on the necessary expansion may be extracted, with some work, from the proof of Lemma A.5. For any piecewise expanding map, such bounds will be satisfied after taking a higher iterate.

<sup>9</sup>The fact that  $\mathcal{L} : \mathcal{H}_p^t(I) \circlearrowright$  is well-defined as a bounded linear operator was established in [5].

$w \mapsto \mathcal{F}^{-1}(m_{-t}\mathcal{F}(w))$  to  $w_j$  yields  $\check{z}_j := \mathcal{F}^{-1}(m_{-t}\mathcal{F}(w_j))$ , a small perturbation of the corresponding smoothed version of  $W_j$ ,  $\check{Z}_j := \mathcal{F}^{-1}(m_{-t}\mathcal{F}(W_j))$ . This approximation is now close in the more basic  $L_q$  norm.

The smoothing procedure described above yields an isometry between  $\mathcal{H}_q^{-t}(\mathbb{R})$  and  $L_q(\mathbb{R})$ . Thus,  $\|\check{Z}_j\|_{L^q} = \|W_j\|_{\mathcal{H}_q^{-t}} \neq 0$ . Hence, provided adequate normalizations are taken, if  $\|\check{z}_j\|_{L^q}$  is very close to zero, one may discard  $w_j$  as an isolated eigenvector. In fact, as we order eigenvectors according to the magnitude of the corresponding eigenvalues, if  $w_j$  is not an isolated eigenvector, neither is any  $w_k$  with  $k \geq j$ . In order to be able to compare the norms of the different eigenvectors, we initially normalize them in the  $L_q$  norm; this is equivalent to considering a so-called triple-norm in the Keller-Liverani setup [30].

By identifying the endpoints of the interval  $I$ , we will regard functions on  $I$  as periodic (on  $\mathbb{T}^1$ ); we point out that the eigenvectors of interest are defined on spaces where pointwise values are irrelevant. We will consider the procedure described above as taking place on a periodic domain. For experiments in dimension two, we will be concerned with tori only, where the definition of fractional Sobolev spaces is an immediate generalization of (13).

The previous discussion suggests the following numerical test.

**Test 1** (Threshold for fractional Sobolev norms). *Set  $0 < t < \frac{1}{p} < 1$  (as in Theorem 3.1), and  $q = (1 - p^{-1})^{-1}$ .*

1. Fix a resolution  $N$  and a number  $0 < k \ll N$ . Compute the top  $k$  right eigenvectors of the Ulam matrix  $\mathcal{L}_N$ ,  $\{w_1, \dots, w_k\}$ , normalized in  $L_q$ .
2. Compute their discrete Fourier transforms  $\{\hat{w}_1, \dots, \hat{w}_k\}$ .
3. Compute the weighted discrete Fourier transforms,  $z'_j(\xi) = \hat{w}_j(\xi)\langle\xi\rangle^{-t/2}$ , where  $\langle\xi\rangle := (1 + |\xi|^2)$ . Set  $z_j(\xi) = z'_j(\xi)(\sin(\pi\xi/N)/(\pi\xi/N))^2$ <sup>10</sup>.
4. Compute the inverse discrete Fourier transforms  $\{\check{z}_1, \dots, \check{z}_k\}$ .
5. Set a threshold  $\tau > 0$ .
6. If  $\|\check{z}_j\|_{L^q}$  is below the threshold  $\tau$ , discard  $w_l$  as an isolated eigenvector for every  $l \geq j$ .

Table 1 illustrates how Test 1 is implemented in Matlab. Such code shows how to compute  $\|\check{z}_j\|_{L^q}$  in Step (6), assuming  $w = w_j$  is a vector of even length  $N$ , normalized in  $q$ -norm.

The smoothing procedure involved in Test 1 also provides a practical tool for identifying almost-invariant sets. Indeed, while stability of Koopman eigenvectors has been established by Theorem 3.1 in a distributional sense, the corresponding stability properties allow us to rely on smoothed versions of the eigenvectors for detecting almost-invariant components. In analogy with the Dellnitz-Froyland ansatz, we will use level sets of the smoothed versions of top eigenvectors to identify almost-invariant sets for the dynamics.

**4.1. One-dimensional piecewise smooth expanding maps.** We will illustrate the use of Test 1 with a family of piecewise smooth expanding maps  $T$ , involving parameters  $\epsilon, \delta$ . This family has been chosen, somewhat arbitrarily, in such a way

<sup>10</sup>The multiplicative factor  $\hat{p}(\xi) := (\sin(\pi\xi/N)/(\pi\xi/N))^2$ , where  $N$  is the resolution, is introduced to recover the approximation to Fourier integrals given by the trapezoid rule. The inverse discrete Fourier transform of  $\hat{p}\hat{F}$  corresponds to the piecewise linear function interpolating the values  $F(n/N)$  at points  $n/N$ ,  $0 \leq n < N$ ,  $n \in \mathbb{N}$  [23, Thm 5.30]. We point out, however, that the outcomes of our experiments with or without this correction are very similar.

```

y = fftshift( fft(w) ); % fftshift swaps the left and right halves of the
                        % vector, so the first entry of fft(w) (zero-
                        % frequency component) moves to the center of y
xi = transpose( -N/2:N/2-1 );
z = y.* ( 1+xi.^2 ).^( -t/2 ) .* ( sin(pi.*xi./N) ./ ( pi.*xi./N )).^2;
z(N/2+1) = y(N/2+1); % to get rid of NaN entry in z
norm( ifft(ifftshift(z)), q )

```

TABLE 1. MATLAB code for the implementation of Test 1.

that when  $\epsilon$  and  $\delta$  are close to 0, the maps are small perturbations of a map with three ergodic components. Thus, for those parameters, it is reasonable to expect (at least) three near-unit isolated eigenvalues, corresponding to metastable components.

Figure 3 depicts two such maps, corresponding to parameters  $\epsilon = .01$  and  $\delta \in \{0.1, 0.2\}$ . As  $\delta$  increases, the leftmost peak moves up, making the two left thirds interact more strongly. The parameter  $\epsilon$  may be regarded as fixed for the rest of this section, and the dependence of the map on the parameters  $\epsilon, \delta$  will not necessarily be explicit. Given parameters  $\epsilon, \delta$ , we let:

$$T(x) = \begin{cases} 2(1 + 3\frac{\delta}{\sqrt{2}})x, & \text{for } x \leq \frac{1}{6} \\ \frac{1}{3} + \frac{\delta}{\sqrt{2}} - 2(1 + 3\frac{\delta}{\sqrt{2}})(x - \frac{1}{6}) + 1000(x - \frac{1}{6})^2(x - \frac{1}{3})^2, & \text{for } \frac{1}{6} < x \leq \frac{1}{3} \\ \frac{4}{9} + (2 + 9\frac{\epsilon}{\sqrt{2}})(x - \frac{1}{3}), & \text{for } \frac{1}{3} < x \leq \frac{4}{9} \\ \frac{1}{2} - (3 + 18\frac{\epsilon}{\sqrt{2}})(x - \frac{1}{2}) + 100000(x - \frac{4}{9})^2(x - \frac{5}{9})^3, & \text{for } \frac{4}{9} < x \leq \frac{5}{9} \\ \frac{1}{3} - \frac{\epsilon}{\sqrt{2}} + (2 + 9\frac{\epsilon}{\sqrt{2}})(x - \frac{5}{9}), & \text{for } \frac{5}{9} < x < \frac{2}{3} \\ 1 - 2(1 + 3\frac{\epsilon}{\sqrt{2}})(x - \frac{2}{3}), & \text{for } \frac{2}{3} \leq x < \frac{5}{6} \\ 1 + 2(1 + 3\frac{\epsilon}{\sqrt{2}})(x - 1), & \text{for } \frac{5}{6} \leq x \leq 1 \pmod{1}. \end{cases} \quad (14)$$

**Remark 4.1** (Choice of parameters for Test 1). *We make the following choices for the remainder of this section. We fix  $p = 1.1$ , as  $p = 1$  would be the limiting case corresponding (almost) to the space of functions of bounded variation, where piecewise smooth expanding maps have been extensively studied. This choice determines  $q = 11$ .*

We set  $t = 0.9$ , which yields rather smooth outcomes for  $\{\check{z}_1, \dots, \check{z}_k\}$ , making more evident the low frequency features of  $\{w_1, \dots, w_k\}$ .

We fix  $k = 5$ , the number of eigenvalues to investigate. For step (5), we choose  $\tau = 0.05$ , corresponding 5% of the norm of the dominant eigenfunction  $w_1 \equiv 1$ .

We point out that Test 1 seems robust under choices of parameters. We have performed experiments with various choices, and arrived to similar conclusions. For example we have tested  $p = q = 2$ , which is commonly used in the applied literature for higher dimensional mixing systems.

**Example 4.2** (Metastable map with 3 components).

Test 1 is illustrated in Figure 5 for the map  $T : I \circlearrowleft$  depicted in Figure 3(a), corresponding to  $\epsilon = .01, \delta = 0.1$ . The left figure shows the eigenvalues of the Ulam matrix of resolution  $2^{13}$  bins; they have been obtained with Matlab's routine `eig`. The right figure shows the quotient of  $\mathcal{H}_q^{-t}$  and  $L_q$  norms of the top 25 eigenvectors, obtained as described in Table 1. We note a transition between the top 3 and the other eigenvectors.

Figures 6 and 7, illustrate the top  $k = 5$  left eigenvectors of two Ulam matrices corresponding to different resolutions ( $N = 2^{12}$  and  $N = 2^{13}$ ). Each row of Figures 6

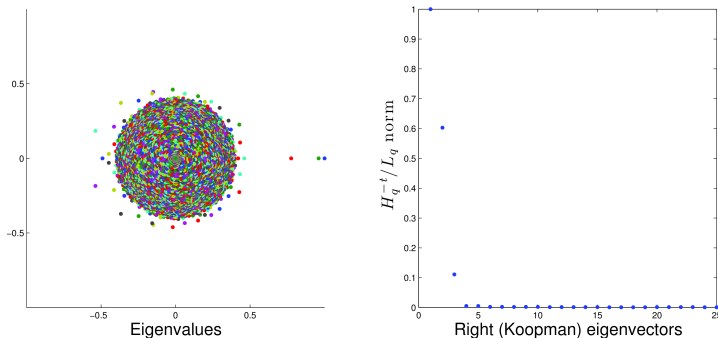


FIGURE 5. Left: Eigenvalues of Ulam matrix of Example 4.2. Right: Fractional Sobolev norms of top 25 right eigenvectors. Resolution:  $2^{13}$  bins.

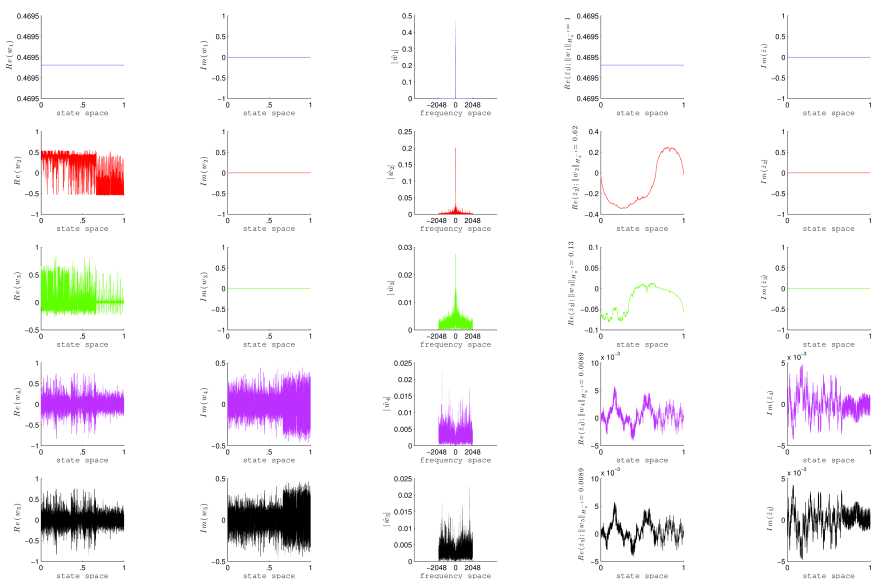
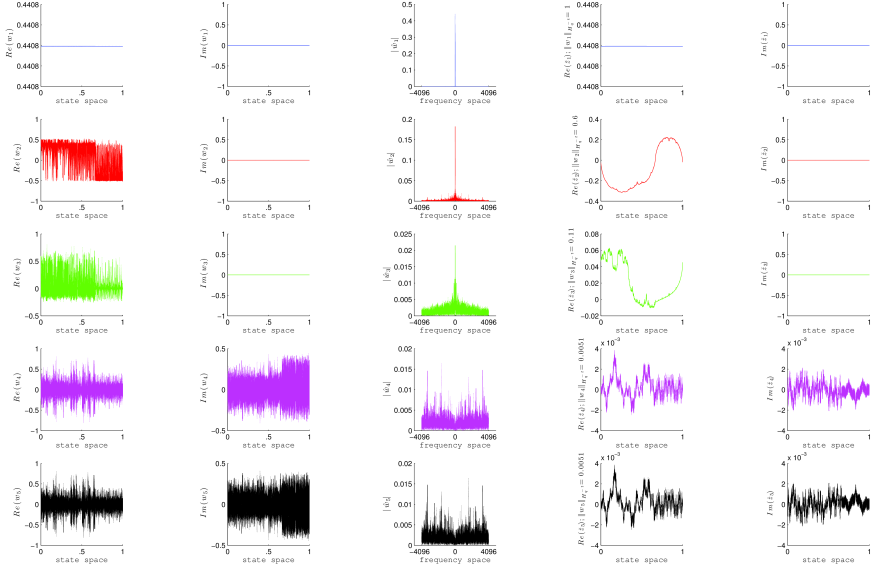
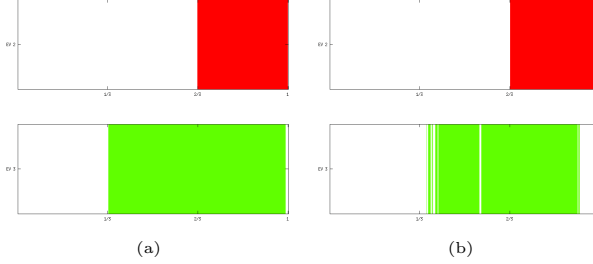


FIGURE 6. Test 1 for Example 4.2: map (14) with  $\epsilon = .01$  and  $\delta = 0.1$ . 1st and 2nd columns: real and imaginary parts of right Ulam eigenvectors  $w_j$ ; 3rd column:  $|\hat{w}_j|$ ; 4th and 5th columns: real and imaginary parts of  $\check{z}_j$ , respectively. Resolution:  $2^{12}$  bins.

and 7 corresponds to a fixed eigenvalue. The first two columns depict real and imaginary parts of right Ulam eigenvectors  $w_j$ , obtained with Matlab routine `eigs`. The third column displays the magnitude of the discrete Fourier transform  $\hat{w}_j$  of  $w_j$ , obtained with `fft` composed with `fftshift`.

Set  $z_j(\xi) = \hat{w}_j(\xi)\langle\xi\rangle^{-t/2}(\sin(\pi\xi/N)/(\pi\xi/N))^2$ . Columns 4 and 5 of Figures 6 and 7 show real and imaginary parts of  $\check{z}_j$ , respectively. The  $\mathcal{H}_q^{-t}$  norm of  $\check{z}_j$  is shown next to the vertical axis of Column 4. Column 4 is a smoothed version of Column 1; similarly, Column 5 is a smoothed version of Column 2. For both resolutions, Test 1 allows us to detect the presence of three isolated eigenvalues for  $\mathcal{L}^*$ . They correspond to those rows for which the fractional Sobolev norms exceed the threshold 0.05.

Figure 8 illustrates how the level sets of smoothed eigenvectors can provide information about almost-invariant components of the underlying map, by setting a

FIGURE 7. As in Figure 6. Resolution:  $2^{13}$  bins.FIGURE 8. Partitions of the interval given by level sets of smoothed 2nd and 3rd eigenvectors of the Koopman operator of (14), with parameters  $\epsilon = .01$  and (a)  $\delta = 0.1$ , (b)  $\delta = 0.2$ . (Obtained from Column 4 of Figures 7 and 10.)

threshold and separating the phase space into parts above and below the threshold. The upper graphs depict the signs of the level sets of the smoothed 2nd eigenvector. The lower graphs show the partitions given by the 3rd eigenvectors, with thresholds 0.034 in (a) and .0025 in (b). While the thresholds are *ad hoc* choices in our examples, the existence of an adequate option already shows the value of the proposed algorithm for the identification of almost-invariant sets. We recall that the partition into intervals  $(0, 1/3)$ ,  $(1/3, 2/3)$  and  $(2/3, 1)$  is invariant for the map with parameters  $\epsilon = 0, \delta = 0$ .

**Remark 4.3.** *We note that the Fourier transforms in the top three rows of Figures 6 and 7, unlike the bottom ones, have their highest peak at low frequencies. This suggests a test for metastability, which has also been robust to different resolutions and maps. (See also Figures 10, 13 and 14.) Intuitively, it is reasonable to consider the dominance of low frequencies as a sign of metastability. However, rigorous arguments substantiating this claim are, to our knowledge, unavailable.*

**Example 4.4** (Collapse of metastable components).

By increasing  $\delta$  from 0 in (14), we can observe a change in the number of metastable components. Let us fix  $\epsilon = .01$  and increase  $\delta = 0.1$  in Example 4.2 to  $\delta = 0.2$ . Figure 9 shows the eigenvalues of the Ulam matrix corresponding

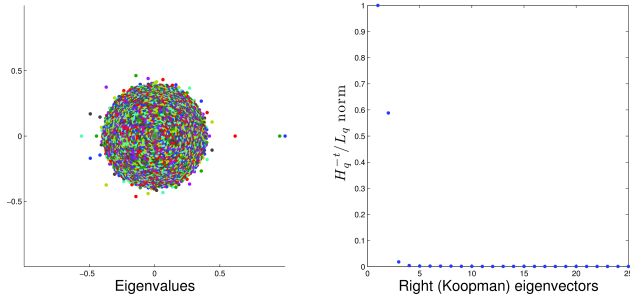


FIGURE 9. Left: Eigenvalues of Ulam matrix of Example 4.4. Right: Fractional Sobolev norms of top 25 right eigenvectors. Resolution:  $2^{13}$  bins.

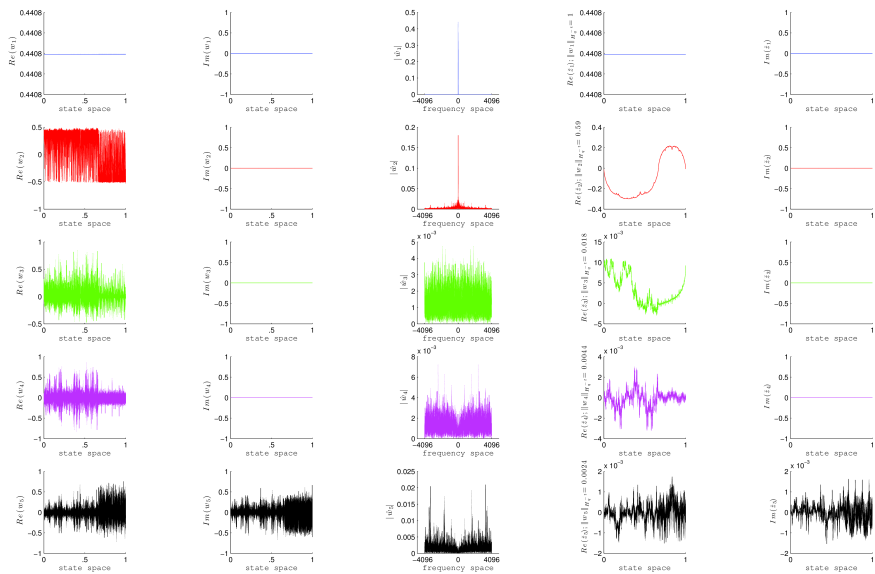


FIGURE 10. Test 1 for Example 4.4: map (14),  $\epsilon = .01, \delta = 0.2$ . Resolution:  $2^{13}$  bins.

to  $2^{13}$  bins (left), and the quotient of  $\mathcal{H}_q^{-t}$  and  $L_q$  norms of the top 25 eigenvectors (right).

This test suggests that the third isolated eigenvalue of Example 4.2 is lost for  $\delta = 0.2$ , as the corresponding Sobolev norm is below the threshold.

Figure 10 illustrates the top 5 right Ulam eigenvectors, as well as their smoothed versions of Test 1. Columns and rows are as explained in Example 4.2. Figure 8(b) has been obtained as Figure 8(a) in the Example 4.2. The top part of Figure 8(b) (red and white online) allows one to distinguish the two almost-invariant components of the underlying system.

#### Example 4.5 (Metastable map with rotation).

We consider the addition of a rotation to the map (14) with parameters  $\epsilon = 0.01$ ,  $\delta = 0.1$ , and define  $T_\theta(x) = T(x) + \theta \pmod{1}$ . When  $\theta = 1/3$ , the three (previously) almost-invariant intervals  $(0, 1/3)$ ,  $(1/3, 2/3)$ , and  $(2/3, 1)$  are now cyclically interchanged by  $T_\theta$ , to become almost-cyclic sets [11]. This property manifests in the spectrum of the Perron-Frobenius operator  $\mathcal{L} : \mathcal{H}_p^t \circlearrowleft$  and Koopman operator  $\mathcal{L}^* : \mathcal{H}_q^{-t} \circlearrowleft$  in the following way. Instead of the eigenvalue 1 and two other real

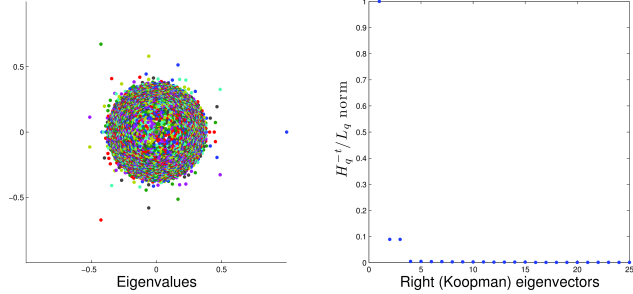


FIGURE 11. Left: Eigenvalues of Ulam matrix of Example 4.5,  $\theta = 1/\pi$ . Right: Fractional Sobolev norms of top 25 right eigenvectors. Resolution:  $2^{13}$  bins.

eigenvalues close to 1 as in Example 4.2, we now have the eigenvalue 1 and the two complex cube roots of unity of magnitude close to 1. The complex eigenfunctions of the two complex-conjugate eigenvalues are rotated by 1/3 forward (resp. backward) by the Perron-Frobenius operator (resp. Koopman operator).

For irrational  $\theta$ , as in the periodic rotation case, the spectrum of the Perron-Frobenius and Koopman operators *may* possess an isolated complex-conjugate pair of eigenvalues. This will occur if the rotation is compatible with the dynamics of  $T$  so that rotating ‘‘coherent sets’’ persist. Denote the complex-conjugate pair of isolated eigenvalues  $\lambda_2 = r_2 e^{i\beta}, \bar{\lambda}_2 = r_2 e^{-i\beta}$ , with corresponding complex eigenfunctions  $f_2, \bar{f}_2$ . Since

$$\mathcal{L}f_2 = r_2(\cos(\beta)\Re(f_2) - \sin(\beta)\Im(f_2)) + ir_2(\sin(\beta)\Re(f_2) + \cos(\beta)\Im(f_2)), \quad (15)$$

and  $\mathcal{L}$  preserves real functions, we see

$$\mathcal{L}(\Re(f_2)) = r_2(\cos(\beta)\Re(f_2) - \sin(\beta)\Im(f_2)) \text{ and } \mathcal{L}(\Im(f_2)) = r_2(\sin(\beta)\Re(f_2) + \cos(\beta)\Im(f_2)).$$

By considering the set  $\mathcal{S} := \{\varrho_\zeta : 0 \leq \zeta < 1\}$ , where  $\varrho_\zeta := \Re(f_2)\cos(2\pi\zeta) - \Im(f_2)\sin(2\pi\zeta)$ , in the case of the Perron-Frobenius operator, one can extract a family of rotating ‘‘coherent sets’’ of the form  $A_\zeta = \{\varrho_\zeta \geq c_\zeta\}, \{\varrho_\zeta < c_\zeta\}$  for suitable threshold  $c_\zeta$  (chosen so that  $\nu(\{\varrho_\zeta \geq c_\zeta\})$  is independent of  $\zeta$ ), where  $\zeta = k\theta, k \in \mathbb{Z}$ . A similar construction applies to the smoothed eigenfunctions of  $\mathcal{L}^*$  by linearity of the Fourier transform.

If  $\theta = 1/\pi$ , the rotation is close to 1/3 and it approximately maintains the structure of the almost-invariant sets  $(0, 1/3), (1/3, 2/3)$ , and  $(2/3, 1)$ . Thus in Figure 11 we see two complex eigenvalues of large magnitude, which appear to be isolated according to Test 1. In contrast if  $\theta = 0.2$ , this rotation does not preserve the collection of almost-invariant sets  $(0, 1/3), (1/3, 2/3)$ , and  $(2/3, 1)$ , and the metastability is lost. In Figure 12, Test 1 indicates the possible presence of only one nontrivial isolated eigenvalue, and correspondingly that the three-set structure is destroyed by this rotation.

Figures 13 and 14 depict eigenvectors and their smoothed versions for  $T_{1/\pi}$  and  $T_{0.2}$ , with rows and columns as explained in Example 4.2. Figure 15(a) depicts positive and negative level sets of the smoothed 2nd eigenvector for  $T_{1/\pi}$ , corresponding to  $\zeta = 0$  and  $\zeta = 1/\pi$ , illustrating the rotating coherent sets discussed above. (In this case, the second eigenvalue of the Ulam matrix is  $\lambda_2 = -0.4256 + 0.6726i$ , which has argument  $\beta \sim 2.1349$ . This approximately corresponds to  $\zeta = 1/\pi$ .) It is worth remarking that this partition clearly encodes large-scale features of the system. Indeed, it is not highly disconnected as it would be for other eigenvectors. Figure 15(b) illustrates the argument of the smoothed 2nd eigenvector for  $T_{1/\pi}$ . The eigenvector condition (15) implies that the action of  $\mathcal{L}$  on the angle is simply a

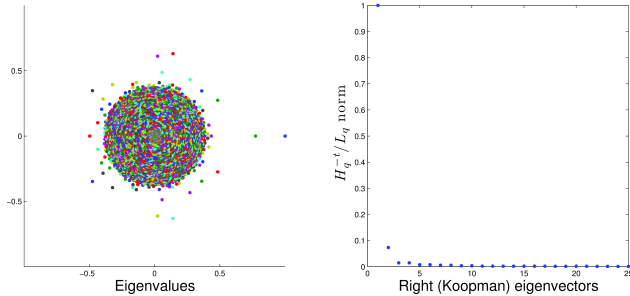


FIGURE 12. Left: Eigenvalues of Ulam matrix of Example 4.5,  $\theta = 0.2$ . Right: Fractional Sobolev norms of top 25 right eigenvectors. Resolution:  $2^{13}$  bins.

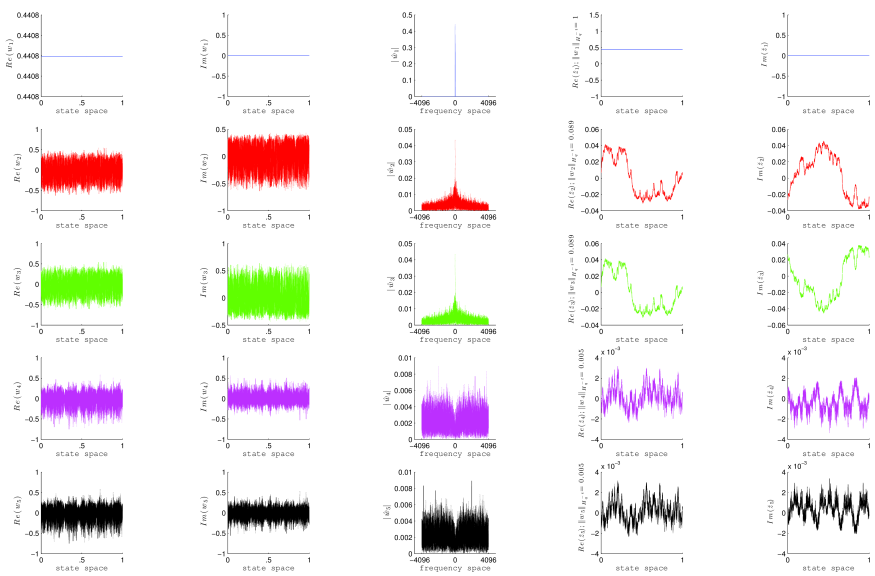


FIGURE 13. Test 1 for Example 4.5: map (14),  $\epsilon = .01, \delta = 0.1, \theta = 1/\pi$ . Resolution:  $2^{13}$  bins.

rotation with argument  $\beta$ . Notice that the inverse image of  $[-\pi/2, \pi/2]$  corresponds to positive real part, so Figure 15(a) could be recovered from Figure 15(b).

**Remark 4.6.** It is worth mentioning that a test analogous to Test 1 can be implemented for eigenvectors of the Perron-Frobenius operator (left eigenvectors of the Ulam matrix). Indeed, the test could consist of steps (1)–(6) of Test 1, with the left Ulam eigenvectors  $v_1, \dots, v_k$  instead of  $w_1, \dots, w_k$ ,  $q$  replaced by  $p$  and  $-t$  by  $t$ . However, such a test roughens eigenfunctions instead of smoothing them. Since numerical approximations introduce noise, at least at small scales, such a roughening procedure emphasizes less-well-approximated modes, and thus provides, in our experience, less reliable outcomes.

**4.2. Two dimensional examples.** In this section, we investigate the application of Test 1 to two-dimensional systems with expanding and contracting directions. We set the parameters  $p = q = 2$  and  $t = 1$ , so that the corresponding Sobolev norm is  $\mathcal{H}_2^{-1} = \mathcal{H}^{-1}$ . Such a norm is used to quantify fluid mixing, and called a mix-norm [34]. It is worth remarking that this norm smooths out high frequency modes in all directions. For this reason, we employ the same norm to measure eigenvectors of

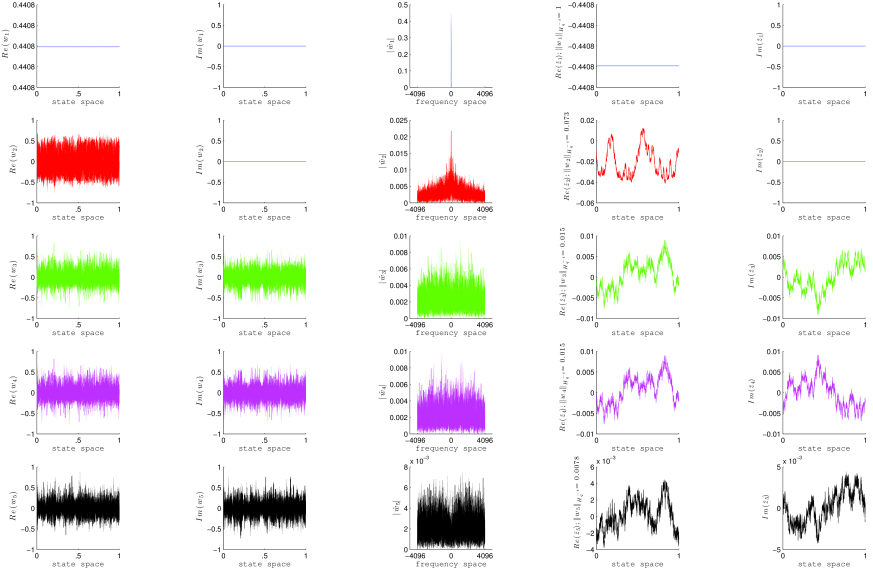


FIGURE 14. Test 1 for Example 4.5: map (14),  $\epsilon = .01$ ,  $\delta = 0.1$ ,  $\theta = 0.2$ .  
Resolution:  $2^{13}$  bins.

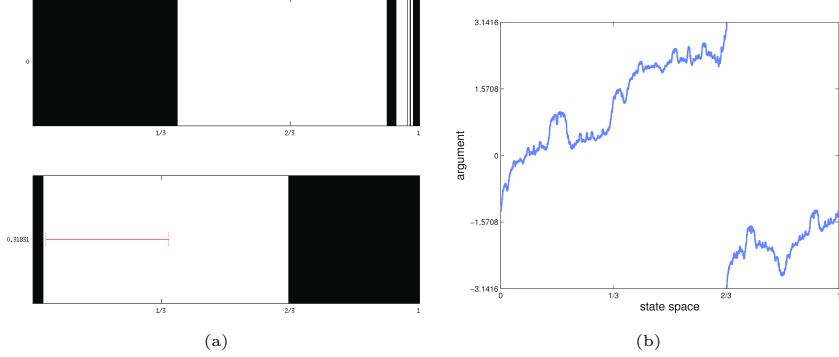


FIGURE 15. (a) Partition into *rotating coherent sets* from smoothed 2nd eigenvector of the Koopman operator of map (14), with parameters  $\epsilon = .01$ ,  $\delta = 0.1$ ,  $\theta = 1/\pi$  and  $\zeta = 0$  (top),  $\zeta = 1/\pi$  (bottom). The horizontal line illustrates the rotation corresponding to  $\zeta = 1/\pi$ . (Obtained from Columns 4 and 5 of Figure 13.) (b) Argument of smoothed 2nd eigenvector.

Perron-Frobenius and Koopman operators. We set threshold  $\tau = 1/3$ . It is worth pointing out that the examples at hand turn out to be highly robust under changes of this value. Indeed, any threshold in the range  $(0.3, 0.7)$  would yield the same conclusions.

We remark that this procedure also allows eigenvectors of the transfer operator to be used to identify almost-invariant sets in the hyperbolic case, and not only in the elliptic case where there are truly invariant sets. This setup has been investigated in [26, 35, 17, 33] and references therein. In related work, [15] proposes the so-called unwrapping procedure. There seems to be a similarity between the plots of

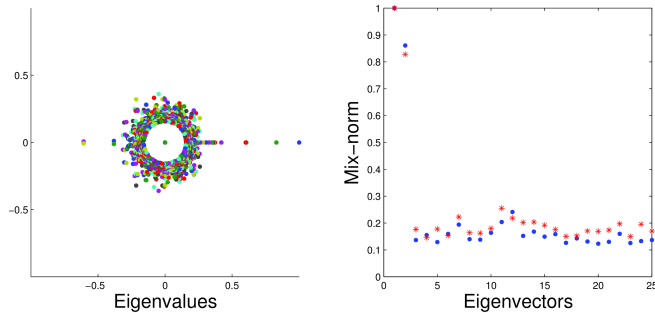


FIGURE 16. Left: Top  $2^{10}$  eigenvalues of Ulam matrix of weakly coupled standard maps (Example 4.7). Right: Mix-norms of left and right eigenvectors (circles and asterisks, respectively).

[15] and the smoothed eigenvectors arising from our experiments. Both methods involve smoothing effects; however, there is at present no complete explanation for these similarities.

**Example 4.7** (Weakly interacting standard maps).

Here we investigate a two-dimensional system obtained from joining two standard maps in a weakly interacting way. More precisely, we study a map on a  $4\pi \times 2\pi$  rectangle, obtained from applying a shift of 5% to the left ( $\text{mod } 4\pi$ ), then applying the standard map on each  $2\pi \times 2\pi$  side, then shifting 5% to the right, and finally reapplying the double standard map on each side. The standard map applied on each side is given by  $(x, y) \mapsto (x+y, y+8 \sin(x+y))$  ( $\text{mod } 2\pi$ ). The horizontal shifts, which only affect the  $x$  coordinate, are determined by  $x \mapsto x \pm 4\pi/20$  ( $\text{mod } 4\pi$ ).

While rigorous results on the spectrum of the transfer operator for this system are not available, we anticipate that Test 1 detects at least two isolated eigenvalues, corresponding to the almost-invariant left and right components of the system.

We analyze the Ulam matrix corresponding to  $256 \times 512$  bins resolution. The top  $2^{10}$  eigenvalues are depicted in Figure 16(a). Here, there seem to be several eigenvalues which could be isolated. The mix-norms of the first 25 eigenvectors are plotted in Figure 16(b). There is a clear gap between the mix-norm of the first two and the rest of the eigenvectors, which is detected by Test 1. Thus, this test adds confidence to the claim that the first two eigenvectors are associated with large-scale dynamical features.

As in the one-dimensional case, the smoothing procedure damps higher Fourier frequencies in such a way that distributions in the space  $\mathcal{H}^{-1}$  get transformed to functions in  $L^2$ . Furthermore, a large  $\mathcal{H}^{-1}$  norm can be interpreted as the presence of a large-scale structure underlying the distribution. Figure 17 shows the top 5 left and right eigenvectors of the Ulam matrix, as well as the corresponding smoothed versions. We observe that the level sets of the smoothed second eigenvectors provide a very good approximation of the almost-invariant left and right halves. It is worth pointing out that the remaining eigenvectors may still encode information about (almost-)invariant sets. However, such sets would correspond to smaller-scale phenomena.

**Example 4.8** (Weakly interacting cat maps).

Next we consider a variant of the previous example: a pair of weakly coupled Arnold's cat maps. More precisely, we study a map on rectangle  $[0, 2] \times [0, 1]$ , obtained from applying a shift of 5% to the left (treating the entire rectangle as a

torus), then applying the double cat map (linear hyperbolic map  $\begin{pmatrix} 2 & 1 \\ 1 & 1 \end{pmatrix}$  map on each  $1 \times 1$  square, treating each half as a torus), then shifting 5% to the right, and finally reapplying the double cat map.

We analyze the Ulam matrix corresponding to  $256 \times 512$  bins resolution. The top  $2^{10}$  eigenvalues are depicted in Figure 18(a). The first 25 values of the mix-norms of left and right eigenvectors are plotted in Figure 18(b). The outcomes of Test 1 again separate the top two isolated eigenvalues, adding confidence to the claim that the first two eigenvectors correspond to large-scale dynamical features. Figure 19 shows the top 5 left and right eigenvectors, as well as the corresponding smoothed versions. The level sets of the smoothed second eigenvectors clearly identify the almost-invariant left and right sides of the phase space. The third row of Figure 19 may encode further almost-invariant sets, corresponding to blue and red in the 2nd and 5th columns. It is not clear whether the system features large-scale almost-invariant sets apart from left and right sides, and the corresponding eigenvector may be interesting for further analyses.

**5. Conclusion.** Transfer operator methods of detecting and identifying metastable dynamics are becoming increasingly pervasive in the analysis of real-world dynamical systems. These methods are based on numerical estimates of the eigenfunctions of the transfer operator (or Koopman operator) that correspond to *isolated* eigenvalues. In this work we put forward the first numerical method for determining *which* of the computed eigenfunctions correspond to isolated eigenvalues. Our numerical approach is based on the expected regularity properties of the computed eigenfunctions, and is supported by a new theoretical result concerning the stability of the isolated spectrum of the transfer operator and its dual, the Koopman operator. Our suggested implementation of the numerical method is based on Fourier analytic tools, which are currently being used in both applied and pure studies of mixing in dynamical systems (under the names of mix-norms and fractional Sobolev spaces, respectively). We show that these tools, in conjunction with the well-known Ulam method of numerically approximating the linear operators, effectively numerically identify isolated spectrum of transfer and Koopman operators, as well as recover underlying large-scale nearly invariant sets. Our proposed numerical test provides an improved visualisation of almost-invariant or metastable sets (an improvement over the raw eigenfunctions of the transfer operator and Koopman operator), particularly in the complicated setting where there is both expanding and contracting dynamics. We also provide an interpretation of eigenprojectors corresponding to complex eigenvalues. The current paper is focused on autonomous systems, and work on extending the method to the non-autonomous setting is underway.

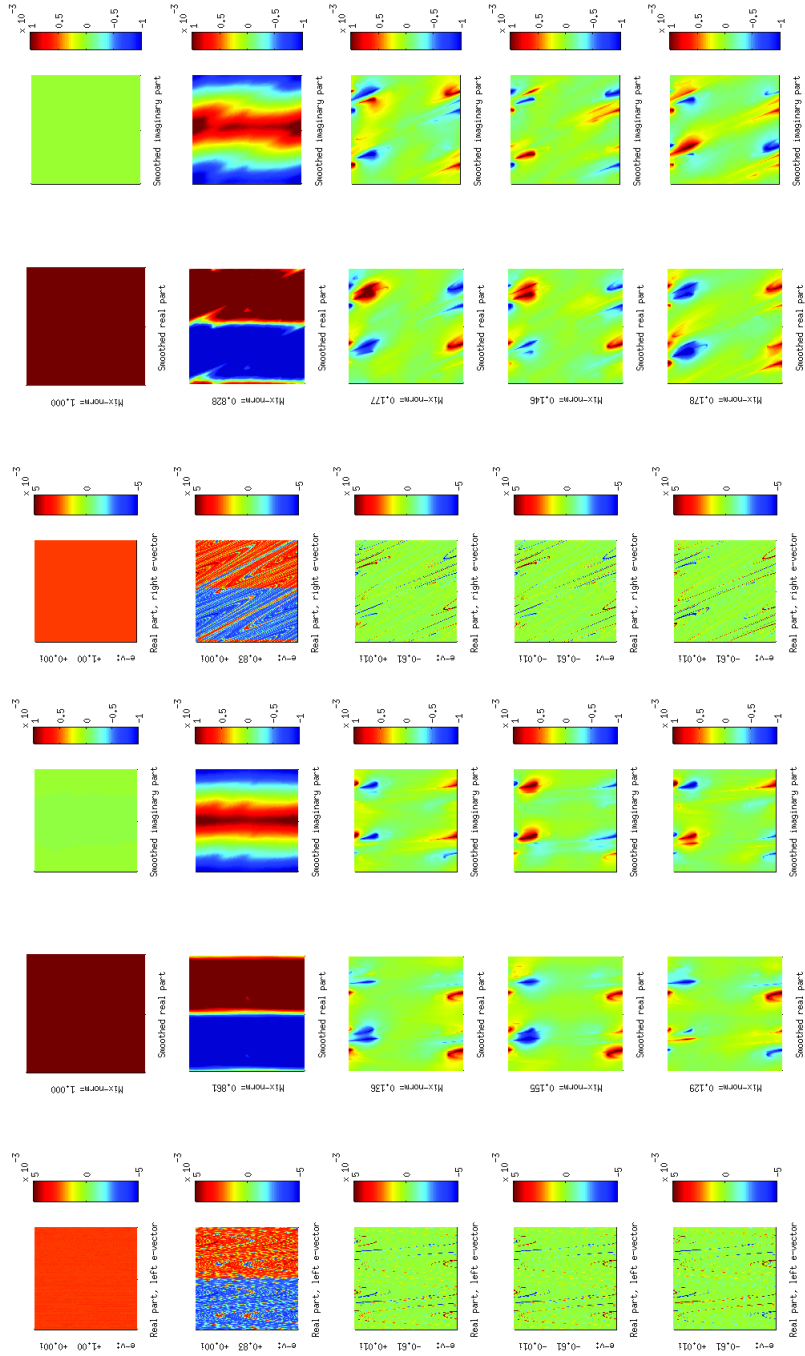


FIGURE 17. Test for weakly coupled standard maps (Example 4.7); figure should be considered in landscape orientation. 1st column: real part of left Ulam eigenvectors, eigenvalues are shown on vertical axis; 2nd and 3rd columns: real and imaginary parts of smoothed left Ulam eigenvectors, mix-norms are shown on vertical axis; 4th column: real part of right Ulam eigenvectors; 5th and 6th columns: real and imaginary parts of smoothed right Ulam eigenvectors. Resolution:  $256 \times 512$  bins.

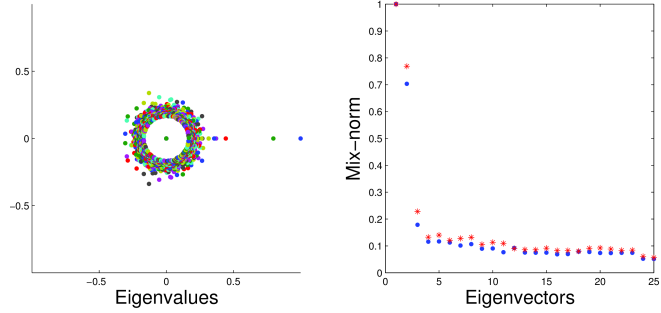


FIGURE 18. Left:  
Top  $2^{10}$  eigenvalues  
of Ulam matrix of  
weakly coupled cat  
maps (Example 4.8).  
Right: Mix-norms  
of left and right  
eigenvectors (circles  
and asterisks,  
respectively).

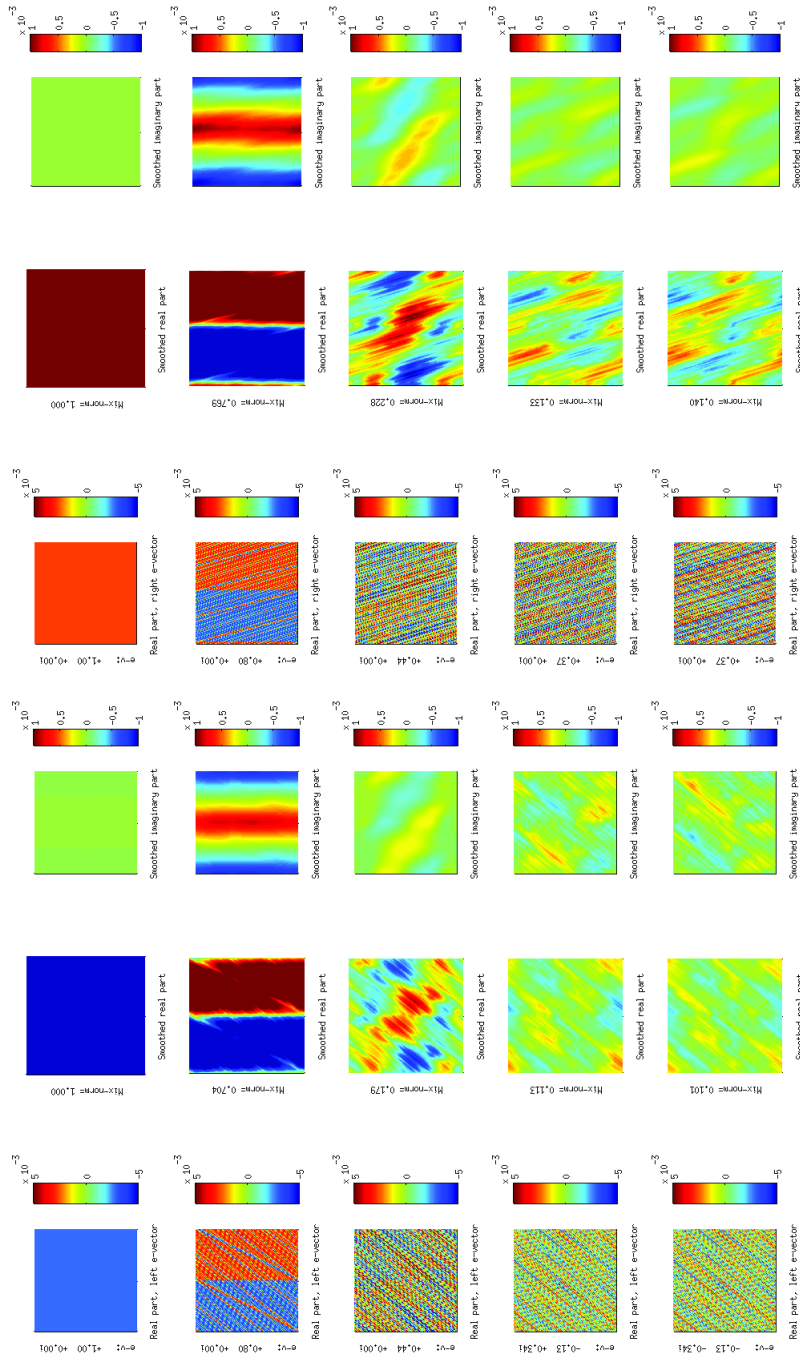


FIGURE 19. Test for weakly coupled cat maps, Example 4.8; figure should be considered in landscape orientation. 1st column: real part of left Ulam eigenvectors, eigenvalues are shown on vertical axis; 2nd and 3rd columns: real and imaginary parts of smoothed left Ulam eigenvectors, mix-norms are shown on vertical axis; 4th column: real part of right Ulam eigenvectors; 5th and 6th columns: real and imaginary parts of smoothed right Ulam eigenvectors. Resolution:  $256 \times 512$  bins.

**Appendix A. Proof of Theorem 3.1.** Throughout this section, we will use  $\|\cdot\|$  and  $|\cdot|$  to denote  $\|\cdot\|_{\mathcal{H}_p^t}$  and  $\|\cdot\|_{\mathcal{H}_p^{t'}}$ , respectively. We will need with some preparatory material.

**A.1. Approximation by smooth functions.** Let  $f \in \mathcal{H}_p^t$  and  $\epsilon > 0$ . Set

$$f_\epsilon := \sum_{j \in \mathbb{Z}} e^{-\epsilon(1+(2\pi j)^2)} a_j \phi_j(x), \quad (16)$$

where  $\phi_j(x) = e^{2\pi i j x}$  and  $a_j := \int_0^1 \phi_j(y) f(y) dy$ . Then,  $f_\epsilon \in C^\infty$ . Since  $|a_j| \leq \|f\|_1$ , a direct calculation shows

$$\|f_\epsilon\|_{C^2} \leq \sum_{j=1}^{\infty} e^{-\epsilon(1+(2\pi j)^2)} (2\pi j)^2 \|f\|_1 \leq C(\epsilon) \|f\|_{\mathcal{H}_p^t}, \quad (17)$$

for some decreasing function  $C : (0, \infty) \rightarrow \mathbb{R}_+$  such that  $\lim_{\epsilon \rightarrow 0^+} C(\epsilon) = \infty$ .

The main result of this subsection is the following approximation lemma.

**Lemma A.1.** *Let  $f \in \mathcal{H}_p^t$ . Then,  $|f_\epsilon - f| \leq C_\# \epsilon^{\frac{t-t'}{2}} \|f\|$ .*

Before proceeding with the proof, we present a lemma about sequences of bounded variation. Let  $b = (b_j)$ , indexed by  $\mathbb{Z}$ . We define its *variation* by  $\text{var}(b) := \sum_{j \in \mathbb{Z}} |b_j - b_{j-1}|$ . Let  $(\phi_j)$  denote the standard orthonormal basis for  $L^2(\mathbb{T})$ . That is,  $\phi_j(x) := e^{2\pi i j x}$ . For a bounded sequence  $b$ , define an operator on  $L^p(\mathbb{T})$  by

$$M_b : \sum_j a_j \phi_j \rightarrow \sum_j a_j b_j \phi_j. \quad (18)$$

**Lemma A.2.** *Let  $b = (b_j)$  be a sequence of non-negative reals such that  $\text{var}(b) < \infty$  and  $b_j \rightarrow 0$  as  $j \rightarrow \pm\infty$ . Then for each  $p > 1$ ,  $\|M_b\|_p \leq C_p \text{var}(b)$ .*

The following auxiliary result will be used in the proof.

**Lemma A.3.** *Let  $(b_j)$  be as in the statement of Lemma A.2. Define sets  $\mathcal{S}_1$  and  $\mathcal{S}_2$  as follows:*

$$\begin{aligned} \mathcal{S}_1 &= \bigcup_j \{j\} \times [0, b_j) \\ \mathcal{S}_2 &= \bigcup_i \bigcup_{j \geq i} (\{i, i+1, \dots, j\} \times [\max(b_{i-1}, b_{j+1}), \min(b_i, b_{i+1}, \dots, b_j)) \}, \end{aligned}$$

Then  $\mathcal{S}_1 = \mathcal{S}_2$  and the union in  $\mathcal{S}_2$  is a disjoint union. Writing  $I_{i,j}$  for

$$[\max(b_{i-1}, b_{j+1}), \min(b_i, b_{i+1}, \dots, b_j)),$$

with the convention that  $[c, d]$  is empty if  $d \leq c$ , and setting  $h_{i,j} = |I_{i,j}|$ , we have  $\sum_{i,j} h_{i,j} = \frac{1}{2} \text{var}(b)$ .

The content of this lemma is illustrated in Figure 20.

*Proof of Lemma A.2.* Consider  $b : \mathbb{Z} \rightarrow [0, \infty)$  as a function on the integers. By Lemma A.3, we can write

$$b = \sum_{i,j} h_{i,j} \mathbf{1}_{[i,j]},$$

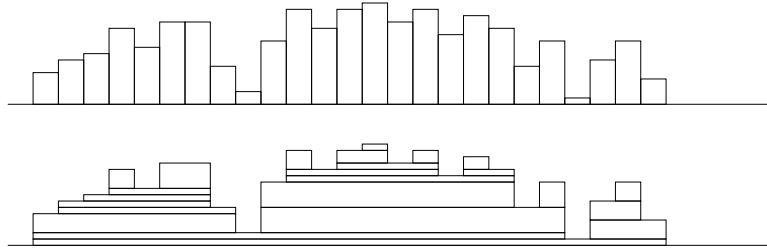


FIGURE 20. Illustration of Lemma A.3.

where  $h_{i,j}$  is given by  $|I_{i,j}|$ , the length of the interval defined in Lemma A.3. In particular, we deduce

$$M_b = \sum_{i,j} h_{i,j} S_{[i,j]},$$

where  $S_{[i,j]}(f) := \sum_{l=i}^j a_l \phi_l$ . Thus,  $\|M_b\|_p \leq \sum_{i,j} h_{i,j} C_p = \frac{1}{2} \text{var}(b) C_p$ , where  $C_p$  is a uniform bound on  $\|S_k\|_p$ , and  $S_k$  is the truncated Fourier series  $S_k(f) := \sum_{|j| \leq k} a_j \phi_j$ .  $\square$

**Corollary A.4.** *Let  $(b_j)$  be as in the statement of Lemma A.2. Suppose  $(b_j)$  is piecewise monotonic with at most  $K$  pieces. Then,  $\|M_b\|_p \leq C_p K \|b\|_\infty$ .*

*Proof of Lemma A.1.* Let  $\epsilon > 0$ , and  $b_{j,\epsilon} = \langle j \rangle^{\frac{t'-t}{2}} (1 - e^{-\epsilon \langle j \rangle})$ . Then,

$$|f - f_\epsilon| = \left\| \sum_{j=1}^{\infty} b_{j,\epsilon} \langle j \rangle^{\frac{t}{2}} \hat{f}(j) \phi_j \right\|_p = \|M_b(J_t f)\|_p \leq \|M_b\|_p \|f\|_{\mathcal{H}_p^t}, \quad (19)$$

where  $M_b$  is the operator defined in (18), and  $J_t : H_p^t(\mathbb{T}) \rightarrow L^p(\mathbb{T})$  is given by  $J_t(f) := \mathcal{F}^{-1} m_t \mathcal{F}(f)$ , with  $m_t(\xi) = \langle \xi \rangle^{\frac{t}{2}} = (1 + |\xi|^2)^{\frac{t}{2}}$ .

For  $0 < \gamma < 1$ , let  $h(x) = x^{-\gamma} (1 - e^{-\epsilon x})$ . One can check that  $h$  has two intervals of monotonicity. For  $x < 1/\epsilon$ , one has  $h(x) \leq \epsilon x^{1-\gamma}$ , while for  $x \geq 1/\epsilon$ , one has  $h(x) \leq x^{-\gamma}$ . In particular, one has  $\|h\|_\infty \leq \epsilon^\gamma$ .

Using the above with  $\gamma = \frac{t-t'}{2}$ , the lemma follows from (19) and Corollary A.4.  $\square$

**A.2. Boundedness of  $\mathbb{E}_k$  in  $\mathcal{H}_p^t$ .** Recall that  $\mathbb{E}_k$  is the conditional expectation with respect to the uniform partition of the interval into  $k$  bins. It is well known that  $\mathbb{E}_k$  is a contraction in  $L_p$ . For  $\mathcal{H}_p^t$  norms, we are not aware of any similar results in the literature. Here we establish the following, which may be of independent interest.

**Lemma A.5.** *Let  $p > 1$  and let  $0 < t < 1/p$ . There exists a constant  $C_\#$  such that  $\|\mathbb{E}_k f\| \leq C_\# \|f\|$  for all  $k \geq 1$  and all  $f \in \mathcal{H}_p^t$ <sup>11</sup>.*

In order to demonstrate this, we shall make use of a theorem of Strichartz [39].

**Theorem A.6** (Strichartz). *Let  $p > 1$  and  $0 < t < 1$ , and  $f : \mathbb{R} \rightarrow \mathbb{R}$  with  $\text{supp } f \subseteq [0, 1]$ . Then  $f \in \mathcal{H}_p^t$  if and only if  $\|f\|_p + \|S_t f\|_p < \infty$  and the implied*

<sup>11</sup>We remind the reader that  $C_\#$  may depend on parameters  $p, t$ , and that  $\|\cdot\|$  denotes  $\|\cdot\|_{\mathcal{H}_p^t}$  throughout this section.

norm is equivalent to the standard  $\mathcal{H}_p^t$  norm, where  $S_t f$  is given by

$$S_t f(x) = \left( \int_0^\infty \frac{dr}{r^{1+2t}} \left( \int_{-1}^1 |f(x+ry) - f(x)| dy \right)^2 \right)^{1/2}. \quad (20)$$

*Proof of Lemma A.5.* We shall use the notation  $A \lesssim B$  to indicate that the quantity  $A$  is bounded by a constant multiple of the quantity  $B$ , where the constant is independent of  $k$  and any function to which the inequality is being applied.

Let  $k$  be fixed (although we ensure that all bounds that we give are independent of  $k$ ). For  $x \in [0, 1]$ , let  $j(x)$  denote the index of the interval to which  $x$  belongs. That is  $j(x) = \lfloor kx \rfloor$ .

We have  $\|\mathbb{E}_k f\|_p \leq \|f\|_p$  so it suffices to show that  $\|S_t(\mathbb{E}_k f)\|_p \lesssim \|S_t f\|_p$ .

We let  $H_r f(x)$  be the outer integrand in  $S_t f(x)$ , that is

$$H_r f(x) = \frac{1}{r^{1+2t}} \left( \int_{-1}^1 |f(x+ry) - f(x)| dy \right)^2. \quad (21)$$

Notice that  $S_t f(x) \leq S_t^{(1)} f(x) + S_t^{(2)} f(x)$ , where

$$\begin{aligned} S_t^{(1)} f(x) &= \left( \int_0^{1/(2k)} H_r f(x) dr \right)^{1/2} \text{ and} \\ S_t^{(2)} f(x) &= \left( \int_{1/(2k)}^\infty H_r f(x) dr \right)^{1/2}. \end{aligned}$$

We start by establishing an inequality that we use several times. Let  $I_j$  denote the interval  $[(j-1)/k, j/k]$ .

**Claim A.7.**

$$\int_0^1 |\mathbb{E}_k f(x) - f(x)|^p dx \lesssim k^{-pt} \int_0^1 dx \left( \int_{2/k}^{3/k} H_r f(x) dr \right)^{p/2}. \quad (22)$$

*Proof.* Let  $x \in [0, 1]$ . If  $\frac{2}{k} \leq r \leq \frac{3}{k}$ , then

$$\begin{aligned} H_r f(x) &\gtrsim k^{1+2t} \left( \int_{-1}^1 |f(x+ry) - f(x)| dy \right)^2 \\ &\gtrsim k^{3+2t} \left( \int_{x-r}^{x+r} |f(s) - f(x)| ds \right)^2 \\ &\geq k^{3+2t} \left( \int_{I_j(x)} |f(s) - f(x)| ds \right)^2 \\ &\geq k^{3+2t} \left( \int_{I_j(x)} |\mathbb{E}_k f(s) - f(x)| ds \right)^2 \\ &= k^{1+2t} |\mathbb{E}_k f(x) - f(x)|^2. \end{aligned}$$

Integrating in  $r$  over the range  $[\frac{2}{k}, \frac{3}{k}]$  and raising to the  $p/2$  power, we obtain

$$|\mathbb{E}_k f(x) - f(x)|^p \lesssim k^{-pt} \left( \int_{2/k}^{3/k} H_r f(x) dr \right)^{p/2},$$

which establishes the claim upon integrating with respect to  $x$ .  $\square$

Notice for later usage that

$$|\mathbb{E}_k f(x) - f(x)| \lesssim k^{-t} S_t^{(2)} f(x). \quad (23)$$

For a function  $f(x)$ , let  $f_j$  denote the value of  $\mathbb{E}_k f$  on the interval  $I_j$ . Recalling definitions (21) and (20) of  $H_r$  and  $S_t$ , the above implies the inequality

$$k^{pt} \int_0^1 |f_{j(x)}(x) - f(x)|^p dx \lesssim \|S_t f\|_p^p. \quad (24)$$

Straightforward modifications also establish the inequality

$$k^{pt} \int_0^1 |f_{j(x)+1}(x) - f(x)|^p dx \lesssim \|S_t f\|_p^p. \quad (25)$$

We now estimate  $S_t^{(2)} \mathbb{E}_k f(x)$ . Letting  $r > 1/(2k)$ , we have

$$\begin{aligned} H_r(\mathbb{E}_k f)(x) &= \frac{1}{r^{1+2t}} \left( \int_{-1}^1 |\mathbb{E}_k f(x+ry) - \mathbb{E}_k f(x)| dy \right)^2 \\ &\lesssim \frac{(f(x) - \mathbb{E}_k f(x))^2}{r^{1+2t}} + \frac{1}{r^{1+2t}} \left( \int_{-1}^1 |\mathbb{E}_k f(x+ry) - f(x)| dy \right)^2. \end{aligned}$$

Hence we have

$$\begin{aligned} S_t^{(2)}(\mathbb{E}_k f)(x) &\lesssim \left( |f(x) - \mathbb{E}_k f(x)|^2 \int_{1/(2k)}^\infty \frac{1}{r^{1+2t}} dr \right)^{1/2} \\ &\quad + \left( \int_{1/(2k)}^\infty \frac{\left( \int_{-1}^1 |\mathbb{E}_k f(x+ry) - f(x)| dy \right)^2}{r^{1+2t}} dr \right)^{1/2} \quad (26) \\ &\sim k^t |f(x) - \mathbb{E}_k f(x)| + (*), \end{aligned}$$

where  $(*)$  denotes the term on the second line of the inequality.

We then estimate  $(*)$  as follows.

$$\begin{aligned} &\int_{-1}^1 |\mathbb{E}_k f(x+ry) - f(x)| dy \\ &= \frac{1}{2r} \int_{x-r}^{x+r} |\mathbb{E}_k f(s) - f(x)| ds \\ &\lesssim \frac{1}{2r} \sum_{\{j : I_j \cap [x-r, x+r] \neq \emptyset\}} \int_{I_j} |\mathbb{E}_k f(s) - f(x)| ds \\ &\leq \frac{1}{2r} \sum_{\{j : I_j \cap [x-r, x+r] \neq \emptyset\}} \int_{I_j} |f(s) - f(x)| ds \\ &\lesssim \int_{-1}^1 |f(x + (r + \frac{1}{k})y) - f(x)| dy, \end{aligned}$$

so that  $(*) \lesssim \left( \int_{1/(2k)}^\infty H_{r+\frac{1}{k}} f(x) dr \right)^{1/2} \leq S_t^{(2)} f(x)$ . Hence, by Theorem A.6 and definition of  $S_t^{(2)} f$ ,  $\|(*)\|_p \lesssim \|f\|_{\mathcal{H}_p^t}$ . Combining this with (26) and (23), we deduce  $\|S_t^{(2)}(\mathbb{E}_k f)\|_p \lesssim \|f\|_{\mathcal{H}_p^t}$ .

It remains to show that  $\|S_t^{(1)}(\mathbb{E}_k f)\|_p \lesssim \|f\|_{\mathcal{H}_p^t}$ . Let  $x = \frac{j}{k} - h$ , where we assume  $h < 1/(2k)$  (the other case being similar). We have  $H_r \mathbb{E}_k f(x) = 0$  if  $r \leq h$  and, recalling that  $r \leq 1/(2k)$ ,  $H_r \mathbb{E}_k f(x) \leq |f_{j+1} - f_j|^2/r^{1+2t}$  if  $r > h$ .

Hence

$$\begin{aligned} S_t^{(1)} \mathbb{E}_k f(x) &\leq |f_{j+1} - f_j| \left( \int_h^{1/(2k)} \frac{1}{r^{1+2t}} dr \right)^{1/2} \\ &\lesssim |f_{j+1} - f_j| h^{-t}. \end{aligned}$$

Integrating the  $p$ th power, we see

$$\begin{aligned} \|S_t^{(1)} \mathbb{E}_k f\|_p^p &\lesssim \sum_j |f_{j+1} - f_j|^p k^{pt-1} \\ &\sim k^{pt} \int_0^1 |f_{j(x)+1} - f_j(x)|^p dx \\ &\sim k^{pt} \left( \int_0^1 |f_{j(x)+1} - f(x)|^p dx + \int_0^1 |f_{j(x)} - f(x)|^p dx \right). \end{aligned}$$

The desired bound then follows from (24) and (25).  $\square$

Another result that will be used later is the following.

**Lemma A.8.** *Let  $g \in C^\gamma$ , with  $t' < \min\{\gamma, \frac{1}{p}\}$ . Then,  $|(\mathbb{E}_k - I)g| \leq C_\# \|g\|_{C^\gamma} \eta_k^{\gamma-t'}$ .*

*Proof.* Let  $g \in C^\gamma$  and  $t < \min(\gamma, 1/p)$ . We will show that  $\|(\mathbb{E}_k - I)g\|_{\mathcal{H}_p^t} \leq C_\# \|g\|_{C^\gamma} k^{t-\gamma}$ .

We use the Strichartz equivalent characterization of  $\mathcal{H}_p^t$  of Theorem A.6 again. Let  $x \in [0, 1]$  be at a distance  $s$  from one of the endpoints of the partition of the interval into subintervals of length  $1/k$ . Let  $g \in C^\gamma$  and let  $h = \mathbb{E}_k g - g$ . We check that  $|h|(z) \leq \|g\|_\gamma k^{-\gamma}$  for all  $z$ .

We have  $\|h\|_{H_t^p} \approx \|h\|_p + \|S_t h\|_p$  where

$$S_t h(x) = \left( \int_0^\infty \frac{dr}{r^{1+2t}} \left( \int_{-1}^1 |h(x+ry) - h(x)| dy \right)^2 \right)^{1/2}.$$

We split the integration over the ranges  $[0, s]$  and  $[s, \infty)$ :

$$\begin{aligned} &\left( \int_0^s \frac{dr}{r^{1+2t}} \left( \int_{-1}^1 |h(x+ry) - h(x)| dy \right)^2 \right)^{1/2} \\ &= \left( \int_0^s \frac{dr}{r^{1+2t}} \left( \int_{-1}^1 |g(x+ry) - g(x)| dy \right)^2 \right)^{1/2} \\ &\leq \left( \int_0^s \frac{dr}{r^{1+2t}} \left( \int_{-1}^1 \|g\|_{C^\gamma} |ry|^\gamma dy \right)^2 \right)^{1/2} \\ &= C_\# \|g\|_{C^\gamma} \left( \int_0^s dr r^{2\gamma-1-2t} \right)^{1/2} \leq C_\# \|g\|_{C^\gamma} k^{t-\gamma}. \end{aligned}$$

Using the uniform bound on  $h$ , we have

$$\left( \int_s^\infty \frac{dr}{r^{1+2t}} \left( \int_{-1}^1 |h(x+ry) - h(x)| dy \right)^2 \right)^{1/2} \leq C_\# \|g\|_{C^\gamma} k^{-\gamma} s^{-t}.$$

Since the  $L^p$  norm of each part is of the form  $C_{\#} \|g\|_{C^\gamma} k^{t-\gamma}$ , the desired result is obtained.  $\square$

**A.3. Proof of Theorem 3.1.** We must verify that the assumptions of Theorem 2.1 are satisfied. The compact embedding condition  $\mathcal{H}_p^t \hookrightarrow \mathcal{H}_p^{t'}$  is established in [4, Lemma 2.2]. The Lasota-Yorke inequality for  $\mathcal{L}$  follows from [5] (or the specialized version in [21]). The uniform Lasota-Yorke inequality for  $\mathcal{L}_n$  follows from Lemma A.5, provided the expansion is sufficiently strong.

It remains to show  $\lim_{k \rightarrow \infty} |(\mathcal{L}_k - \mathcal{L})f| = 0$  for every  $f \in \mathcal{H}_p^t$ . Let  $\eta_k = \frac{1}{k}$  be the diameter of the partition elements of  $\mathcal{P}_k$ . Let  $f \in \mathcal{H}_p^t$ , and for each  $\epsilon > 0$ , let  $f_\epsilon$  as in (16). For each  $k \in \mathbb{N}$ , we have

$$|(\mathcal{L}_k - \mathcal{L})f| \leq |(\mathcal{L}_k - \mathcal{L})f_\epsilon| + |(\mathcal{L}_k - \mathcal{L})(f_\epsilon - f)| =: (U1) + (U2). \quad (27)$$

We will bound each term separately. The fact that

$$(U2) \leq C_{\#} \epsilon^{\frac{t-t'}{2}} \|f\| \quad (28)$$

follows from Lemma A.1, after recalling that  $|\mathbb{E}_k|$  is bounded independently of  $k$ , by Lemma A.5.

Now we estimate (U1). Let  $\{I_i\}_{1 \leq i \leq \beta}$  be the partition of  $I$  into domains of differentiability of  $T$ ,  $Q_i = T(I_i)$ , and  $\xi_i := (T|_{I_i})^{-1}$ . Then, the transfer operator  $\mathcal{L}$  is given by

$$\mathcal{L}f = \sum_{i=1}^{\beta} 1_{Q_i} \cdot f \circ \xi_i \cdot |D\xi_i|.$$

This is the sum of at most  $\beta$  terms of the form  $1_J g$ , where  $J \subset I$  is an interval, and  $g = f \circ \xi_i \cdot |D\xi_i|$  for some  $i \in \mathbb{N}$ . Furthermore, when  $f \in C^\gamma$ , each such  $g$  is also  $C^\gamma$ , and  $\|g\|_{C^\gamma} \leq C \|f\|_{C^\gamma}$ , where  $C$  depends on  $T$ , but not on  $f$ . In this case,  $\mathcal{L}f$  may be rewritten as

$$\mathcal{L}f = (\mathcal{L}f)^h + (\mathcal{L}f)^s,$$

where  $(\mathcal{L}f)^h \in C^\gamma$  is such that  $\|(\mathcal{L}f)^h\| \leq C \|f\|_{C^\gamma}$ , and  $(\mathcal{L}f)^s$  is the sum of at most  $2\beta$  step functions, with jumps of size at most  $\beta \|f\|_\infty$ . Then,  $\|(\mathcal{L}f)^s\|_\infty \leq 2\beta^2 \|f\|_\infty$  and

$$(U1) = |(\mathbb{E}_k - I)\mathcal{L}f_\epsilon| \leq |(\mathbb{E}_k - I)(\mathcal{L}f_\epsilon)^h| + |(\mathbb{E}_k - I)(\mathcal{L}f_\epsilon)^s| =: (U11) + (U12).$$

Let us estimate the first term. Lemma A.8, combined with the bound on  $\|f_\epsilon\|_{C^\gamma}$  implied by (17), immediately yields

$$(U11) \leq C_{\#} \|(\mathcal{L}f_\epsilon)^h\|_{C^\gamma} \eta_k^{\gamma-t'} \leq C_{\#} C \|f_\epsilon\|_{C^\gamma} \eta_k^{\gamma-t'} \leq C(\epsilon) \|f\| \eta_k^{\gamma-t'}. \quad (29)$$

For the second term, we note that  $(\mathbb{E}_k - I)(\mathcal{L}f_\epsilon)^s$  is a step function with at most  $2\beta$  steps with non-zero value. Also, the change of variables formula shows that for each interval  $J \subset I$ , one has  $|1_J| \leq C_{\#} m(J)^{\frac{1}{p}-t'}$ . Hence, recalling that  $\|(\mathcal{L}f)^s\|_\infty \leq 2\beta^2 \|f\|_\infty$ , we get

$$(U12) \leq 4\beta^3 \|f_\epsilon\|_\infty \sup_{1 \leq j \leq k} |1_{B_k}| \leq C_{\#} \beta^3 \|f_\epsilon\|_\infty \eta_k^{\frac{1}{p}-t'} \leq C_{\#} \beta^3 C(\epsilon) \|f\| \eta_k^{\frac{1}{p}-t'}, \quad (30)$$

where the last inequality follows once again from (17).

Combining (28), (29) and (30) into (27), we get

$$|(\mathcal{L}_k - \mathcal{L})f| \leq C_{\#} \left( \beta^3 C(\epsilon) \eta_k^{\left( \min(\gamma, \frac{1}{p}) - t' \right)} + \epsilon^{\frac{t-t'}{2}} \right) \|f\|, \quad (31)$$

where  $\beta$  is the uniform bound on number of branches of  $T$ . Choosing  $\epsilon$  such that  $\beta^3 C(\epsilon) \leq \eta_k^{-\frac{1}{2}(\min(\gamma, \frac{1}{p}) - t')}$  ensures that  $\lim_{k \rightarrow \infty} |(\mathcal{L}_k - \mathcal{L})f| = 0$ , as claimed.

**Acknowledgments.** The authors are grateful to Michael Dellnitz for motivating us to develop techniques to numerically determine the peripheral spectrum of transfer operators, and to Ben Goldys for useful discussions regarding function spaces.

## REFERENCES

- [1] W. Bahsoun and S. Vaienti, Metastability of certain intermittent maps, *Nonlinearity*, **25** (2012), 107–124, URL <http://dx.doi.org/10.1088/0951-7715/25/1/107>.
- [2] V. Baladi, Unpublished, 1996.
- [3] V. Baladi, *Positive transfer operators and decay of correlations*, vol. 16 of Advanced Series in Nonlinear Dynamics, World Scientific Publishing Co. Inc., River Edge, NJ, 2000, URL <http://dx.doi.org/10.1142/9789812813633>.
- [4] V. Baladi, Anisotropic Sobolev spaces and dynamical transfer operators:  $C^\infty$  foliations, in *Algebraic and topological dynamics*, vol. 385 of Contemp. Math., Amer. Math. Soc., Providence, RI, 2005, 123–135.
- [5] V. Baladi and S. Gouëzel, Good Banach spaces for piecewise hyperbolic maps via interpolation, *Ann. Inst. H. Poincaré Anal. Non Linéaire*, **26** (2009), 1453–1481, URL <http://dx.doi.org/10.1016/j.anihpc.2009.01.001>.
- [6] M. Blank, G. Keller and C. Liverani, Ruelle-Perron-Frobenius spectrum for Anosov maps, *Nonlinearity*, **15** (2002), 1905–1973, URL <http://dx.doi.org/10.1088/0951-7715/15/6/309>.
- [7] M. Budišić, R. Mohr and I. Mezić, Applied Koopmanism, *Chaos: An Interdisciplinary Journal of Nonlinear Science*, **22**, URL <http://scitation.aip.org/content/aip/journal/chaos/22/4/1063/1.4772195>.
- [8] J. Buzzi, No or infinitely many a.c.i.p. for piecewise expanding  $C^r$  maps in higher dimensions, *Comm. Math. Phys.*, **222** (2001), 495–501, URL <http://dx.doi.org/10.1007/s002200100509>.
- [9] W. J. Cowieson, Absolutely continuous invariant measures for most piecewise smooth expanding maps, *Ergodic Theory Dynam. Systems*, **22** (2002), 1061–1078, URL <http://dx.doi.org/10.1017/S0143385702000627>.
- [10] M. Dellnitz, G. Froyland and S. Sertl, On the isolated spectrum of the Perron-Frobenius operator, *Nonlinearity*, **13** (2000), 1171–1188, URL <http://dx.doi.org/10.1088/0951-7715/13/4/310>.
- [11] M. Dellnitz and O. Junge, On the approximation of complicated dynamical behavior, *SIAM J. Numer. Anal.*, **36** (1999), 491–515, URL <http://dx.doi.org/10.1137/S0036142996313002>.
- [12] M. F. Demers and C. Liverani, Stability of statistical properties in two-dimensional piecewise hyperbolic maps, *Trans. Amer. Math. Soc.*, **360** (2008), 4777–4814, URL <http://dx.doi.org/10.1090/S0021-9947-08-04464-4>.
- [13] D. Dolgopyat and P. Wright, The diffusion coefficient for piecewise expanding maps of the interval with metastable states, *Stoch. Dyn.*, **12** (2012), 1150005, 13, URL <http://dx.doi.org/10.1142/S0219493712003547>.
- [14] G. Froyland, R. Murray and O. Stancevic, Spectral degeneracy and escape dynamics for intermittent maps with a hole, *Nonlinearity*, **24** (2011), 2435–2463.
- [15] G. Froyland, Unwrapping eigenfunctions to discover the geometry of almost-invariant sets in hyperbolic maps, *Phys. D*, **237** (2008), 840–853, URL <http://dx.doi.org/10.1016/j.physd.2007.11.004>.
- [16] G. Froyland, S. Lloyd and A. Quas, A semi-invertible Oseledets theorem with applications to transfer operator cocycles, *Discrete Contin. Dyn. Syst.*, **33** (2013), 3835–3860, URL <http://dx.doi.org/10.3934/dcds.2013.33.3835>.
- [17] G. Froyland and K. Padberg, Almost-invariant sets and invariant manifolds—connecting probabilistic and geometric descriptions of coherent structures in flows, *Phys. D*, **238** (2009), 1507–1523, URL <http://dx.doi.org/10.1016/j.physd.2009.03.002>.
- [18] G. Froyland, K. Padberg, M. England and A.-M. Treguier, Detection of coherent oceanic structures via transfer operators, *Phys. Rev. Lett.*, **98** (2007), 224503.

- [19] G. Froyland and O. Stancevic, Escape rates and Perron-Frobenius operators: open and closed dynamical systems, *Discrete Contin. Dyn. Syst. Ser. B*, **14** (2010), 457–472, URL <http://dx.doi.org/10.3934/dcdsb.2010.14.457>.
- [20] C. González-Tokman, B. Hunt and P. Wright, Approximating invariant densities of metastable systems, *Ergodic Theory and Dynamical Systems*, **31** (2011), 1345–1361, URL <http://dx.doi.org/10.1017/S0143385710000337>.
- [21] C. González-Tokman and A. Quas, A semi-invertible operator Oseledets theorem, *Ergodic Theory and Dynamical Systems*, **34** (2014), 1230–1272, URL [http://journals.cambridge.org/article\\_S0143385712001897](http://journals.cambridge.org/article_S0143385712001897).
- [22] P. Góra, A. Boyarsky and H. Proppe, On the number of invariant measures for higher-dimensional chaotic transformations, *J. Statist. Phys.*, **62** (1991), 709–728, URL <http://dx.doi.org/10.1007/BF01017979>.
- [23] G. Gripenberg, Fourier analysis, 2009, Lecture Notes.
- [24] H. Hennion, Sur un théorème spectral et son application aux noyaux lipchitziens, *Proc. Amer. Math. Soc.*, **118** (1993), 627–634, URL <http://dx.doi.org/10.2307/2160348>.
- [25] F. Hofbauer and G. Keller, Ergodic properties of invariant measures for piecewise monotonic transformations, *Math. Z.*, **180** (1982), 119–140, URL <http://dx.doi.org/10.1007/BF01215004>.
- [26] O. Junge, J. Marsden and I. Mezic, Uncertainty in the dynamics of conservative maps, in *Decision and Control, 2004. CDC. 43rd IEEE Conference on*, vol. 2, 2004, 2225–2230 Vol.2.
- [27] T. Kato, Perturbation theory for nullity, deficiency and other quantities of linear operators, *J. Analyse Math.*, **6** (1958), 261–322.
- [28] T. Kato, *Perturbation theory for linear operators*, Classics in Mathematics, Springer-Verlag, Berlin, 1995, Reprint of the 1980 edition.
- [29] G. Keller, On the rate of convergence to equilibrium in one-dimensional systems, *Comm. Math. Phys.*, **96** (1984), 181–193, URL <http://projecteuclid.org/getRecord?id=euclid.cmp/1103941781>.
- [30] G. Keller and C. Liverani, Stability of the spectrum for transfer operators, *Ann. Scuola Norm. Sup. Pisa Cl. Sci. (4)*, **28** (1999), 141–152, URL [http://www.numdam.org/item?id=ASNSP\\_1999\\_4\\_28\\_1\\_141\\_0](http://www.numdam.org/item?id=ASNSP_1999_4_28_1_141_0).
- [31] G. Keller and C. Liverani, Rare events, escape rates and quasistationarity: some exact formulae, *J. Stat. Phys.*, **135** (2009), 519–534, URL <http://dx.doi.org/10.1007/s10955-009-9747-8>.
- [32] G. Keller and H. H. Rugh, Eigenfunctions for smooth expanding circle maps, *Nonlinearity*, **17** (2004), 1723–1730.
- [33] Z. Levnajić and I. Mezić, Ergodic theory and visualization. i. mesochronic plots for visualization of ergodic partition and invariant sets, *Chaos: An Interdisciplinary Journal of Nonlinear Science*, **20** (2010), –, URL <http://scitation.aip.org/content/aip/journal/chaos/20/3/10.1063/1.3458896>.
- [34] G. Mathew, I. Mezić and L. Petzold, A multiscale measure for mixing, *Phys. D*, **211** (2005), 23–46, URL <http://dx.doi.org/10.1016/j.physd.2005.07.017>.
- [35] I. Mezić and A. Banaszuk, Comparison of systems with complex behavior, *Physica D: Non-linear Phenomena*, **197** (2004), 101 – 133, URL <http://www.sciencedirect.com/science/article/pii/S0167278904002507>.
- [36] M. Rychlik, Bounded variation and invariant measures, *Studia Math.*, **76** (1983), 69–80.
- [37] B. Saussol, Absolutely continuous invariant measures for multidimensional expanding maps, *Israel J. Math.*, **116** (2000), 223–248, URL <http://dx.doi.org/10.1007/BF02773219>.
- [38] C. Schütte, A. Fischer, W. Huisenga and P. Deuflhard, A direct approach to conformational dynamics based on hybrid Monte Carlo, *J. Comput. Phys.*, **151** (1999), 146–168, URL <http://dx.doi.org/10.1006/jcph.1999.6231>, Computational molecular biophysics.
- [39] R. S. Strichartz, Multipliers on fractional Sobolev spaces, *J. Math. Mech.*, **16** (1967), 1031–1060.
- [40] J.-L. Thiffeault, Using multiscale norms to quantify mixing and transport, *Nonlinearity*, **25** (2012), R1, URL <http://stacks.iop.org/0951-7715/25/i=2/a=R1>.
- [41] M. Tsujii, Piecewise expanding maps on the plane with singular ergodic properties, *Ergodic Theory Dynam. Systems*, **20** (2000), 1851–1857, URL <http://dx.doi.org/10.1017/S0143385700001012>.
- [42] S. M. Ulam, *A collection of mathematical problems*, Interscience Tracts in Pure and Applied Mathematics, no. 8, Interscience Publishers, New York-London, 1960.

Received xxxx 20xx; revised xxxx 20xx.

*E-mail address:* [g.froyland@unsw.edu.au](mailto:g.froyland@unsw.edu.au)

*E-mail address:* [ceciliagt@unsw.edu.au](mailto:ceciliagt@unsw.edu.au)

*E-mail address:* [aquas@uvic.ca](mailto:aquas@uvic.ca)